spoor

Pilot Report

Spoor - AI Avian Monitoring with CCTV Cameras on Floating Wind Turbines

Experiences and Future Potential

May 2023 - February 2024

Summary

Location: Hywind Tampen Floating Windfarm Norway

Number of cameras: Three

Days of data analysed:195

Hours of video analysed: 3,202

Total bird observations: 1,455

Bird classification:

- 1,309 (90%) classified to order level
- 1,293 (89%) classified to family level
- 724 (50%) classified to species level

Red list *endangered* birds identified: Black-legged kittiwake

Red list *vulnerable* birds identified: European Herring Gull

spoor

Table of contents

Introduction

Equinor and Spoor have partnered to deploy and evaluate Spoor AI bird-monitoring technology on Hywind Tampen, filling the data gap for accurate, verifiable, high-volume and long-term data on bird activity offshore. These data are potentially hugely valuable in reducing project risk and ensuring that offshore wind is planned and operated in environmentally responsible ways.

Uniquely, this project uses AI to process videos from CCTV cameras which are pre-installed on the floating wind turbine service platforms (originally to monitor operational activities). This innovative configuration means that greater value can be captured from the same hardware performing two different functions. Although the CCTV cameras are lower resolution (and therefore range) than the cameras which Spoor typically uses, this project has the potential to enable the collection of bird-activity and ID data from any and all offshore assets which have CCTV cameras installed. This would enable a rapid scaling of bird activity data-gathering offshore which has the potential to make a huge contribution to the state of the science and of the offshore wind industry worldwide. This pilot is intended to explore the viability hypothesis.

The primary purpose of this report is to document the technical performance of Spoor's solution, and describe its potential nature-positive impact when applied at scale. Analysis of the biodiversity data itself is not the primary purpose.

Hywind Tampen

Hywind Tampen is the largest floating wind farm in the world, located 140 km off the Norwegian coast, (see Figure 1) with a capacity of 88MW, provided by eleven 8.6MW Siemens Gamesa wind turbines. The project directly reduces emissions from oil and gas production on the Snorre and Gullfaks offshore fields by 200,000 tonnes of CO_2 and 1,000 tonnes of NOx emissions per year.

Hywind Tampen is Norway's first full scale offshore wind farm and has a critically important role to play in the development of the Norwegian offshore wind industry and the global expansion of floating offshore wind, which Equinor pioneered. From a biodiversity perspective, Hywind Tampen provides a unique opportunity to gather bird activity data off the coast of Norway and start building a knowledge base to understand and protect vulnerable species as they interact with industrial windfarm development.

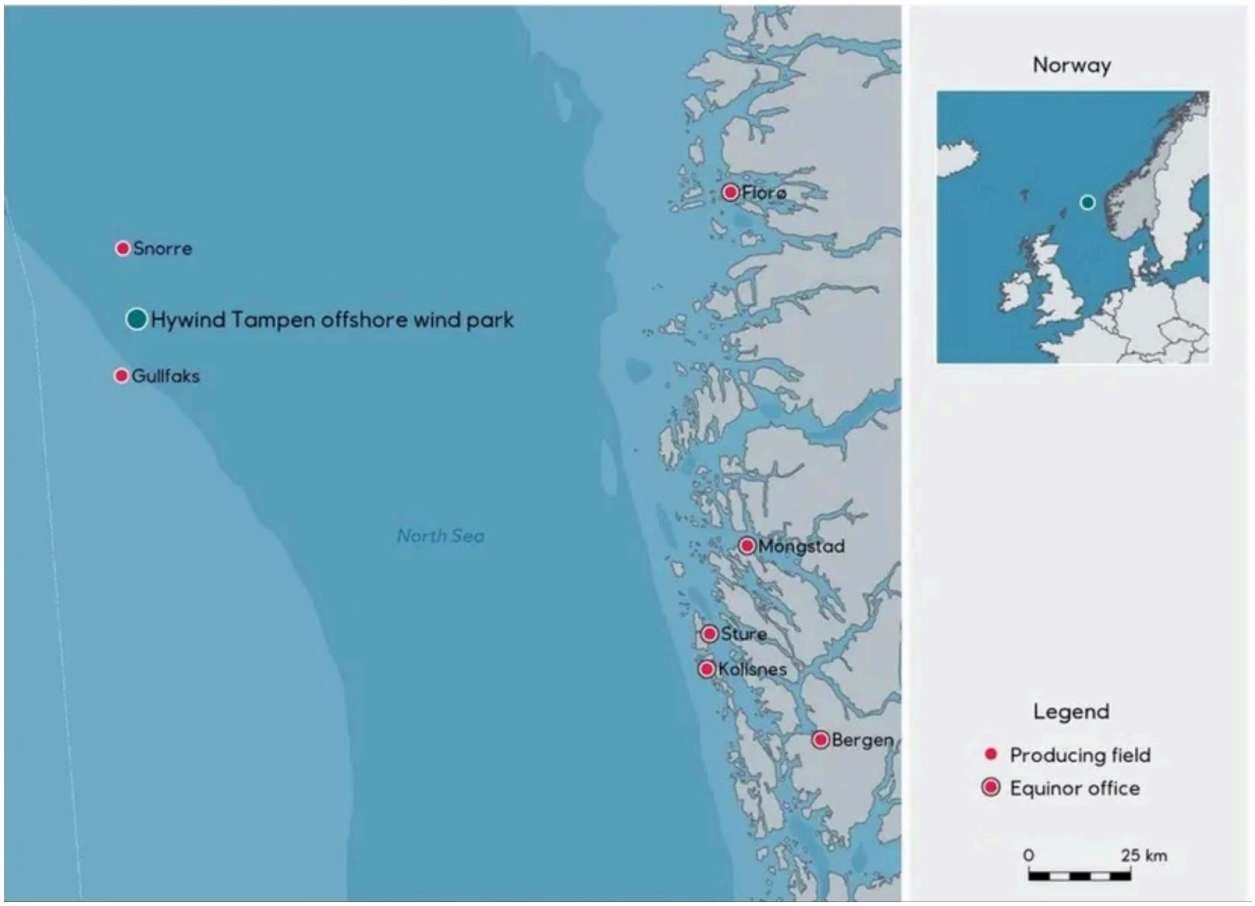

Figure 1: Courtesy of Equinor: Hywind Tampen (n.d)*, showing the location of the Hywind Tampen wind farm, 140 km off the Norwegian west coast.*

About Spoor

Spoor is a Norwegian biodiversity technology company, with a vision to enable nature and industry to coexist. Spoor promotes biodiversity positive wind energy development by combining high-resolution video cameras with advanced AI-based software to detect, track and identify birds and analyse their activity. This kind of accurate, detailed empirical data can reduce environmental and financial risks and allow smarter decision making by developers and regulators. Spoor currently employs 22 people of diverse backgrounds; with 14 nationalities and a 36% female representation. The team's expertise includes ornithology, offshore wind, regulatory affairs, data science, edge computing, and machine learning. Since the first pilot was launched in March 2021, Spoor's solution has been deployed on multiple onshore and offshore sites in Northern Europe, with further installations underway. Together with Equinor and Fugro in a separate project, Spoor pioneered the use of floating offshore platforms offshore to monitor bird-activity for pre-construction surveys.

Bird detection and tracking

The Spoor AI

Spoor's Artificial Intelligence (AI) software analyses all recorded hours of video in order to detect and track birds. Any bird appearing for more than 1 second in the camera field of view is detected and tracked. The output is a video combined with a visual image of the flight trajectory, and several still images of the bird at certain times during the flight. In addition, statistics on temporal distribution, flight height, species, flight directions, and abundance correlated to wind speed and direction are available to users in the Spoor AI webapp (app.spoor.ai).

At the time of writing, Spoor AI software has been trained to identify individual birds. If several birds appear simultaneously in the field of view - either in a flock, or because they happen to be active in the field of view at the same time - the AI will detect and display their separate flight paths. Furthermore, the current Spoor AI has been trained to detect birds in flight, and not birds which are resting or moving at ground level or on the water surface.

AI performance: accuracy, precision and recall

Within machine learning and artificial intelligence, quality is defined by "accuracy", as explained in *Evidently AI: Accuracy vs. precision vs. recall in machine learning: what's the difference?* (n.d). Simply put, it expresses how often the AI is correct. Correct detections are birds that the AI marked as "bird", and non-birds (e.g. an airplane) that the AI marked as "non-bird". These are called true positives and true negatives, respectively. Incorrect detections are birds that the AI marked as "non-bird", and non-birds that the AI marked as "bird". These are called false negatives and false positives, respectively. Accuracy is calculated by dividing the sum of correct (true) detections by the sum of all detections (false and true).

Precision is an expression of how often the AI is correct when it claims to have detected a bird. It is calculated by the number of true positives divided by all positives. Recall is the percentage of the birds the AI manages to detect. Recall is calculated by dividing the number of true positives by the sum of true positives and false negatives, and is discussed in more detail in the *Comparing to a Ground Truth* chapter.

In theory, all the three metrics can reach 100%, but in practice, this is very rarely the case. In most real-life situations, there is for example a tradeoff between optimising precision and optimising recall. Optimising for precision means requiring the AI to be correct almost every time it marks an observation as "bird". In order to achieve a high precision, the AI may disregard observations it is less certain about, with the potential result that a larger number of real birds were marked as "non-bird". The recall is the measure of how many real birds the AI detects, so a higher number of real birds marked as "non-bird" will negatively affect the recall metric.

The definition of a good accuracy level within machine learning depends on the context. Both precision and recall are useful to understand different aspects of the AI. Still, Accuracy is commonly used as the primary quality metric.

Reasons for false detections

False (incorrect) detections are birds that the AI marked as "non-bird", and non-birds that the AI marked as "bird". These are called false negatives and false positives, respectively. The reason for false negatives (birds being missed) are discussed more in the *Comparing to a Ground Truth* chapter. False positives are sometimes called *noise*, and can be insects or other moving objects that resemble the movement of a distant bird, like airplanes or helicopters. Other phenomena that can be interpreted as a bird by the AI are sun reflections on impurities on the lens and certain cloud formations. The reason for these false detections is connected to the specific identifiers that the AI has been trained to recognize, and is constantly improved due to the self-learning nature of the AI.

Quality assurance

In order to ensure high levels of quality, Spoor deploys a number of techniques.

- Spoor prioritises building high-quality AI training data sets. Due to the increasing number of on-site deployments, Spoor has a large and varied asset of raw data. The raw data are processed and refined into unique, high-quality training data sets that feed into the AI. Data processing and refinement is done with advanced tools combined with the biological expertise of Spoor's in-house ornithologist.
- The AI assigns a confidence to detections. If the confidence drops below a certain threshold, the data is manually verified by trained members of staff. Due to the self-learning nature of the AI system, the confidence levels increase over time.
- Several times per week, a sample of all new detections are sent for manual verification in order to monitor the general levels of false and true positives. The self-learning nature of the AI ensures that the level of false positives diminish over time.
- Spoor also conducts regular in-field verifications to measure false negatives. See more in the Comparing to a Ground Truth chapter below.

Comparing to a ground truth

Spoor conducts quality verifications by comparing Spoor AI results to the field observations of human observers (trained ornithologists). This is done at different sites to ensure quality is measured across various environments.

In this method, the human observer visits a site and manually records bird detections within a field of view that match the field of view of the camera used for Spoor data collection.

The bird detections are noted down with information on: time of the bird entering the field of view and exiting the field of view, the bird's trajectory through the field of view, and its species. If

the verification focus is spatial mapping, the human observer records flight height and distance from the observation point. In order for this to be precise, the ornithologist uses an instrument like a laser rangefinder or binoculars with rangefinders. This data set represents a "Ground Truth"; information that is known to be real or true, provided by direct observation and measurement (i.e. empirical evidence).

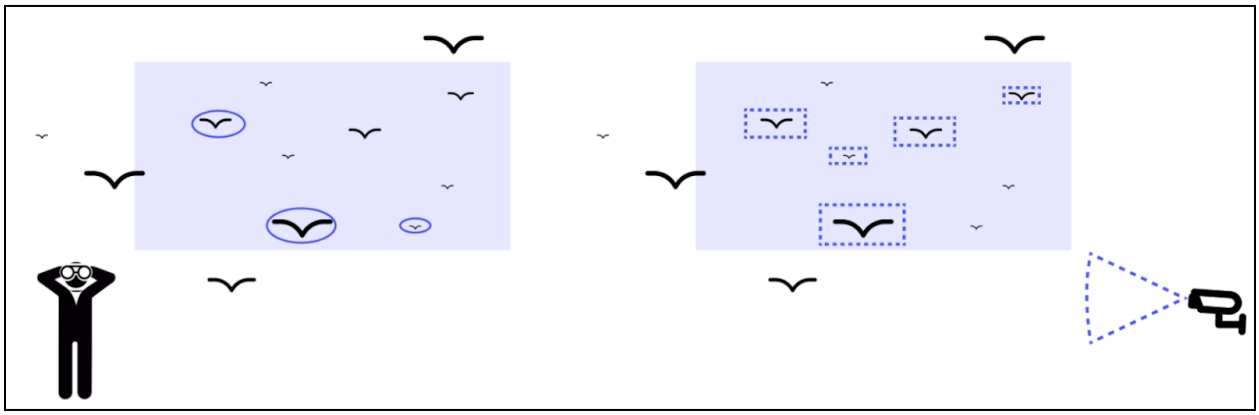

Figure 2: Combining the results of a manual observer (left) and the Spoor AI (right) yields a Ground Truth dataset that can be used for assessing the performance of both the manual observer and Spoor AI.

The Ground Truth dataset is compared with the Spoor AI detections. Because the human observer is also subject to errors, some birds are missed by the human observer but are detected by the Spoor AI. The number of birds missed by humans are determined in the comparison, and added to the Ground Truth data set. This yields a "more true" ground truth than would be achieved by only taking the manual observations as the ground truth. In this way, it serves as a cross-verification of both the Spoor AI and the manual observer, allowing for assessing quality and levels of error of both methods.

Spoor AI compared to an ornithologist

In 2023, Spoor's ornithologist conducted 5 field trips on 4 different onshore sites in Norway and observed for a total of 18.5 hours. Spoor has compared the results of the Spoor AI to the results of the ornithologist, and the results are presented in Table 3. Spoor AI reaches the same recall as the ornithologist; the average is 70% and 71%, respectively. Weighted by duration, the Spoor weighted average recall is 75% with a standard deviation of 12 percent points and the manual weighted average recall is 76% with a standard deviation of 9 percent points.

When the ornithologist recall was higher than Spoor AI recall, the reason was that the AI missed occasional birds that were part of flocks. Due the inherent self-learning properties of the AI combined with Spoor's focus on quality assurance, these results will continuously improve. The birds that the ornithologist missed were to a larger degree single birds that appeared alone. The reason why a manual observer misses birds is mainly due inattention, weariness or focus on other tasks like recording a previous observation.

Site	Field Trip Date	Duration	Ground Truth Detections	Human Detections	Spoor AI Detections	Manual Recall	AI Recall
Site A							
Site A							
Site X							
Site Y							
Site Z							
	Summary	18.5 h	381	271	266	**71%**	**70%**

Table 1: Results from 5 field trips of a human observer, compared to the results of the Spoor AI. The Ground Truth column contains the number of unique bird observations by the human observer and the Spoor AI combined. Human Detections are the number of observations by the human, while Spoor AI detections are the number of observations recorded by the Spoor AI.

Sampling method

Spoor's method is based on observations in a predetermined spatial frame of reference, called Eulerian sampling as explained in Phillips *et al*. (2019). One effect of the Eulerian reference frame is that one cannot track individuals as they leave the reference frame. Each time a bird enters the field of view, it is counted as one observation, and it is not possible to determine whether this individual has been observed before or not. A high number of bird observations does not automatically equal a high abundance of birds. In other words, it is measuring activity levels rather than actual abundance. This is an inherent feature of both a stationary and a moving observer regardless of technology; be it camera-based, manual observer or radar. It is simply an effect of the reference frame of monitoring being a particular spatial volume,or of the bird population as such. If individual birds or a detailed population study is the focus, then bio-logging methods such as bird-ringing/GPS tracking could provide excellent data, which combined with AI camera data could provide unique insights into bird movement and behaviour. Bio-loggins is an example of Lagrangian sampling. Both Eulerian and Lagrangian approaches are vulnerable to uncertainty and/or bias in measurement and sampling.

Range, area and volume

An inherent effect of any observation method based on electromagnetic radiation, is that larger objects are detectable over longer distances than smaller objects. This applies to devices like visual spectrum and thermal cameras, radars, telescopes, and the human eye. Intuitively, we know that the leaf of a tree is a small object that is only visible over a few metres with the

human eye, while the moon is a very large object that is visible over hundreds of thousands of kilometres.

For this reason, large birds are detectable over a longer distance than smaller birds. When discussing detection range, bird size needs to be taken into account.

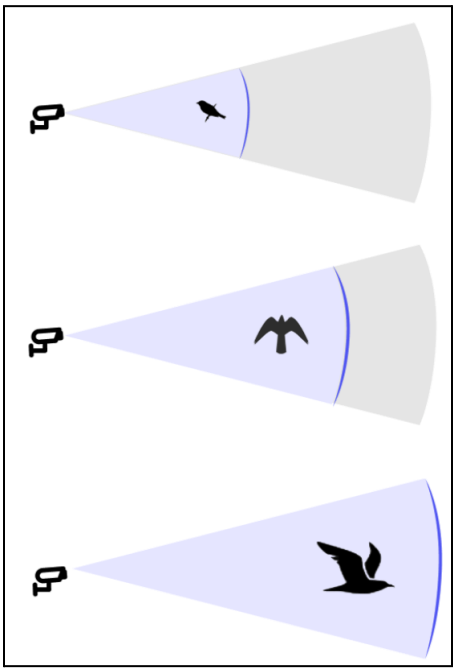

Figure 3: The detection range depends on a number of variables, including the size of the observed birds. In general, large birds are detectable over a longer distance than smaller birds.

The maximum detection range also depends on the properties of the sensor equipment. For a mid-range camera with a standard lens, a bird with a wingspan of 150 cm (like a Great Black-Backed Gull) can in theory be detected up to 2 km away, while a bird with a 25 cm wingspan (like a Meadow Pipit) can be detected up to 350 metres away. Increasing the lens zoom capabilities and/or the camera resolution will yield greater ranges.

Because the purpose of the monitoring in most cases is to get consistent data on bird activity and behaviour within a space, it is not only the range (distance), but also the volume that is important. The surveyed space is a function of the range, height and width of the camera field of view. The effective volume - like range - depends on the bird size and camera properties and settings. The volume can be increased by increasing the range, but also by increasing the height and width of the field of view by selecting appropriate lens types and camera settings.

Flight height, distance and direction

For single-camera sampling, the location of a bird can be derived from an image with both altitude and lateral and longitudinal position, based on the size of the bird and its relative location within the image. The bird size is derived using an average measure for the size of the species it belongs to. For example, the body size of a Great Black-Backed Gull is 64-78 cm

long, with a wingspan of 150-165 cm, according to *The Royal Society for the Protection of Birds: Great Black-backed Gull (n.d.)*.

In general, the uncertainty in the position is driven by a combination of factors such as pixelation (a property of the camera), variation in body size within each species and variation in body orientation.

The bird size can be estimated by using an approximate average bird size. This is the current method used by Spoor, but it includes a larger uncertainty because the true bird size varies between species; from just a few centimetres to more than two metres in wingspan. The uncertainty in the bird size translates into a less accurate spatial position. As a next step, Spoor can calculate spatial positions per bird species, thus greatly reducing the measurement uncertainty.

Flight height can be used to inform the risk of bird collisions with a turbine. Spoor provides a distribution of the flight height of the observed birds, where the height is given in metres above sea level. The space monitored by a conventional camera has a pyramid-like shape, as indicated by the purple area in Figure 4. The flight height of birds being tracked through this volume can be represented in numerous ways. For the purpose of this report, Spoor has chosen to represent flight heights as the number of birds intersecting a vertical cross-section in the middle of the field of view, illustrated as the blue plane in Figure 4.

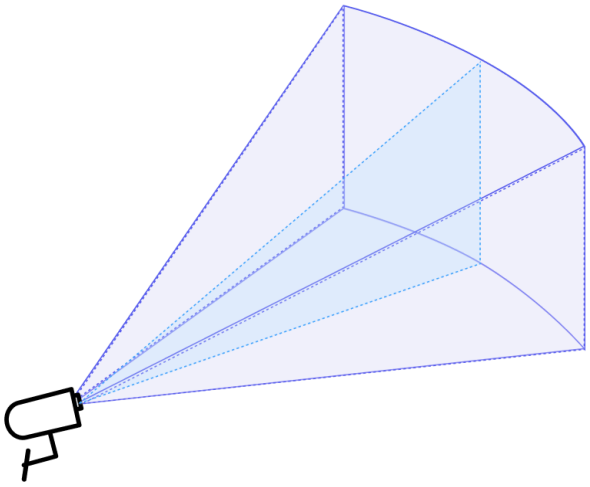

Figure 4: An illustration of the field-of-view volume (purple) and the cross-section (blue), where bird intersections are counted and used for flight height analysis.

The bird intersections are grouped into height bins of 5 metre heights, as illustrated by the black horizontal lines on the blue plane in Figure 5. Due to the triangular shape of the field of view, the area of each height bin varies. In order to have the same unit of measurement across the height bins, Spoor uses the flux metric; measuring *count of bird intersections per* m^2.

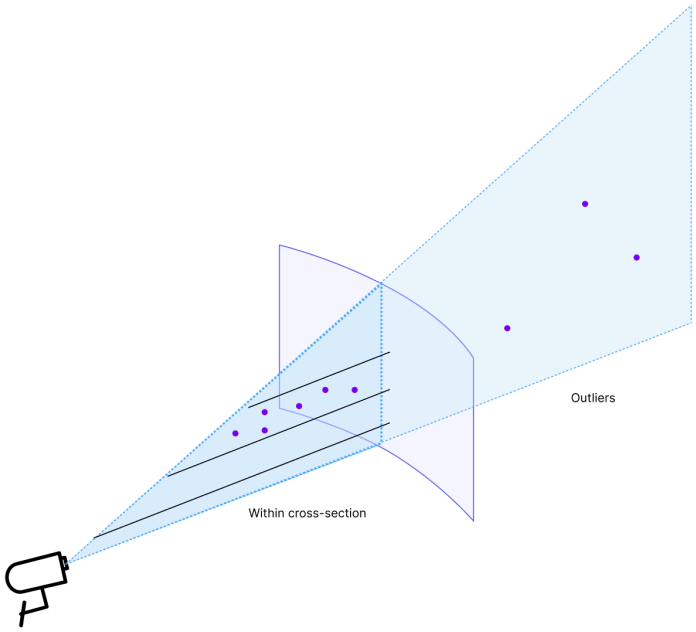

Figure 5: Bird intersections of the cross-section in the middle of the field of view (blue) are illustrated as purple dots. Each intersection is grouped into height bins of 5 metre heights. Any bird observation outside of the defined area is considered as outliers, and is not included in the flight height analysis.

Further, in order to know the precise surveyed area per height bin, Spoor has defined a cutoff distance as illustrated by the purple frame in Figure 5. The distance is equal to the maximum theoretical detection distance for a bird of wing span of 1 metre. Any bird observed beyond this cutoff distance is considered an outlier and is not included in the flight height analysis.

Spoor considers this approach a representative approximation of total distributions of flying heights.

Directionality

The flight direction of each bird is currently calculated as the movement between the first second compared to the last second of the flight path. The bird track is required to be visible for 4 seconds or more. With a lower duration, a flight direction is not calculated. If a bird enters and exits the field of view in the same direction, it is not represented in the flight direction statistics. The unit used for flight direction is compass degrees, but is translated to cardinal and intercardinal directions for simplicity. Cardinal directions are north (N), south (S), east (E) and west (W), while the intercardinal directions are northeast (NE), southeast (SE), southwest (SW), and northwest (NW). Further work could aim at distinguishing more on less linear flight patterns, allowing for analysis to differentiate directions of migratory movements from other activities e.g. foraging or resting.

Taxonomic classifications

The taxonomy levels considered in this report are: order, family and species. The genus level has not been considered.

Classification is done by analysing the full-length track of the bird in question. The duration of a bird track can be from a few seconds and up to the full duration of a video segment (five minutes). In order to determine the taxonomy of detected birds, some type of unique characteristic needs to be exhibited and visible. Unique characteristics can be the visual appearance of the bird (e.g. body, wing or tail shape, colours and patterns), flight characteristics (e.g. flight pattern, flight height, speed, flock behaviour, flapping frequency), and/or environmental factors (e.g. time of day, light or wind conditions). This imitates the way human observers classify birds.

There is no set level of frames needed in order to classify a bird, because the ease and speed of classification depends on the camera properties, visibility and bird characteristics. Some birds are easy to identify due to distinct characteristics which can be observed over large distances. Gulls, common swifts and European Starlings are examples of families and species that exhibit such "long-range" characteristics . Other birds have identifiers that require closer inspection. For example, certain species within the gull family exhibit very similar characteristics, and differentiating these requires higher resolution and/or closer proximity. This is also true for classification by human observers.

The White-tailed Eagle is a species that exhibits unique characteristics in appearance, and Spoor AI has been trained to identify this species. New species will be trained according to demand.

Method

Data capture

Surveillance cameras as sensors

Spoor AI utilises cameras as sensors for data capture. Spoor AI software is hardware agnostic and can process video from any commercially available high-resolution camera. This allows for flexible, lightweight and cost-effective infrastructure. The AI software is adapted to analyse data from both stable and unstable (floating turbines/buoys) vantage points.

Camera-based monitoring is a non-intrusive technology that will not interfere with any other installations. It is also a non-intrusive *methodology* that has minimal interference with the environment and species it is monitoring, and therefore introduces a minimum of sampling biases compared to human observers.

To date, Spoor has worked with surveillance video cameras from multiple manufacturers with both wide-angle dome cameras and classic bullet cameras. Surveillance cameras are affordable and are designed to record continuously for years at a time. They have custom built water and weatherproof housings that are durable in tough weather conditions. One current disadvantage is that they are designed for security rather than scientific purposes, so that certain settings (like focus and focal length, frame rate per second, multi-camera time syncs) are simplified and need to be adjusted by Spoor's engineers. However, both these settings and the general quality and performance of the cameras are being improved by the camera manufacturers on a continuous basis.

The choice of camera, lens, housing and other equipment is decided on a case-by-case basis. Various aspects like cost, durability in different environments, focal distance, and field of view need to be considered in relation to the project specific purpose of monitoring.

A number of variables within the equipment determine the ability and quality of bird detection, some examples being sensor resolution, focal length, lens "speed" (f-stop), shutter speed, frame rate (Frames Per Second, FPS), and data bitrates.

Using cameras for data capture yields both advantages and limitations. Some of the limitations are:

- Visible Imaging Sensor cameras cannot detect without daylight. For 24 hour monitoring they can be combined with thermal imaging cameras.
- Image quality is affected by weather; fog, rain and snow will typically reduce the range. Direct sun striking an unclean lens can also degrade the image quality. In addition, atmospheric quality like humidity, airborne dust or air pollution affects image quality especially onshore.

- Range is ultimately restricted by the physics of lenses and the stability of the mounting location. The longer the focal length, the more likely it is that any vibration will degrade the final video image (e.g. from wind against the camera body, or the vibration of a working wind turbine).

In addition to cameras, a power supply is needed for them in order to function, and a network connection is needed for data transmission. In certain cases where internet access is not available, data needs to be stored onsite and manually retrieved at a later date.

The Hernis CCTV cameras

This pilot used three outdoor CCTV cameras mounted on three floating wind turbines. The cameras had originally been selected for the purpose of HSE monitoring of personnel doing operational and maintenance work on the turbines.

Figure 6: The Hernis CCTV camera, illustration retrieved from Hernis (n.d.)

The CCTV cameras were manufactured by Hernis (see Figure 6). They have resolution of 1920x1080 pixels, a 30x optical zoom lens (4.5-135 mm focal lengths), and a frame rate of 30 frames per second. The view angle is between 2.35° and 65.1°. The cameras have wipers to clean the lens for water and other contamination. The settings and camera orientations can be remotely controlled and adjusted.

Vantage points and camera settings

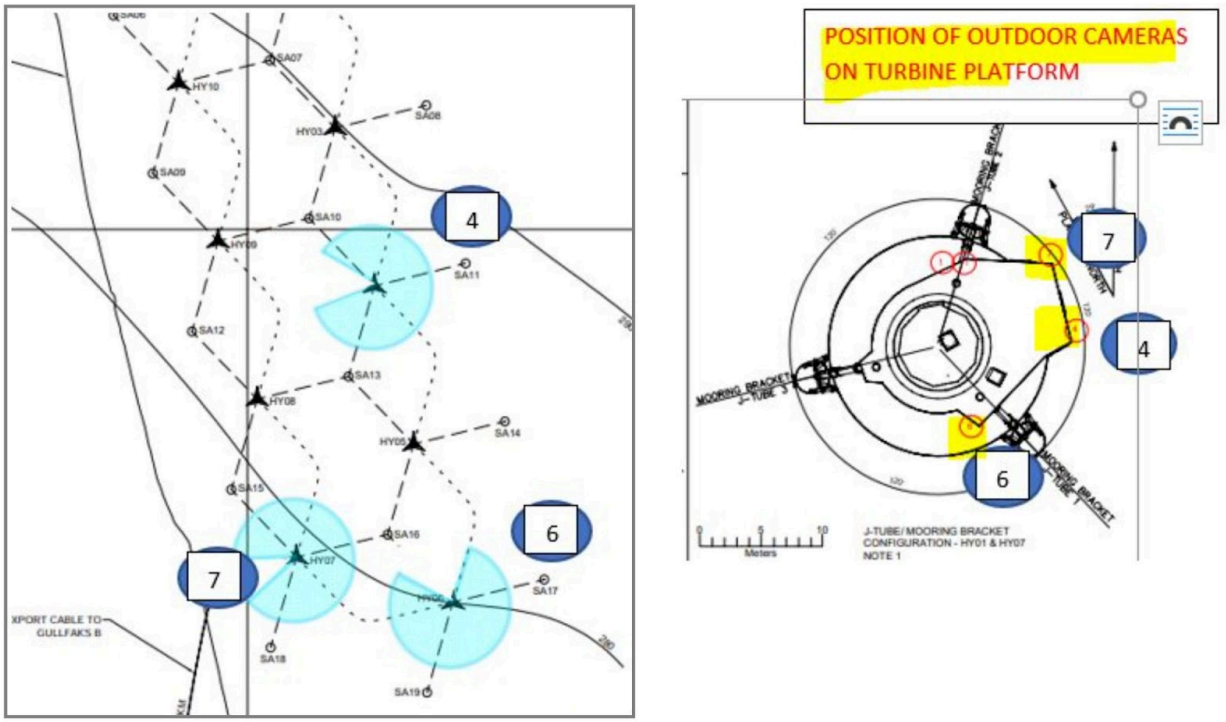

Figure 7: The vantage points of the outdoor CCTV cameras for each of the three turbines in question. The light blue circles indicate the potential field of view. For certain angles, the turbine tower obstructs the view.

The CCTV cameras at Hywind Tampen have been installed for the purpose of HSE monitoring of human operations at the turbine, and the vantage points were selected to optimise for this, and not for bird monitoring – but remote control made it possible to use the cameras for both purposes. In addition, camera placement needs to adhere to safety regulations and should not interfere with turbine operations. The placement of the cameras on the three turbines are shown in Figure 7.

The exact position of each camera is measured by the yaw, pitch and roll angles, as seen in Figure 8.

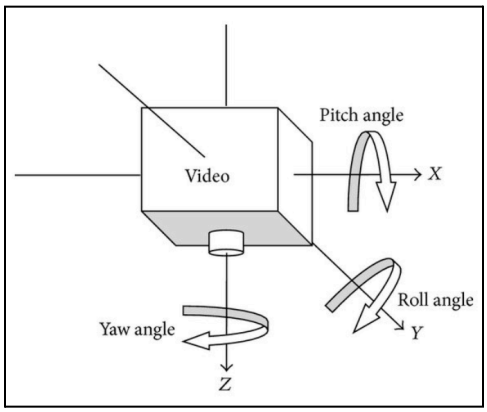

Figure 8: The yaw, pitch and roll angles that describe the position of a camera. Illustration from Zhang *et al*. (2014).

Spoor estimated the yaws, pitches and rolls of each camera based on landmarks visible in the images .These estimates were confirmed as reasonable by Equinor.

The cameras are mounted outside the railing on the turbine platform, as seen in Figure 9. This allows for orienting the camera towards the sea to optimise for bird monitoring, when they are not used for HSE monitoring. Figure 10 shows examples of the camera positions used for HSE monitoring and for bird monitoring, respectively.

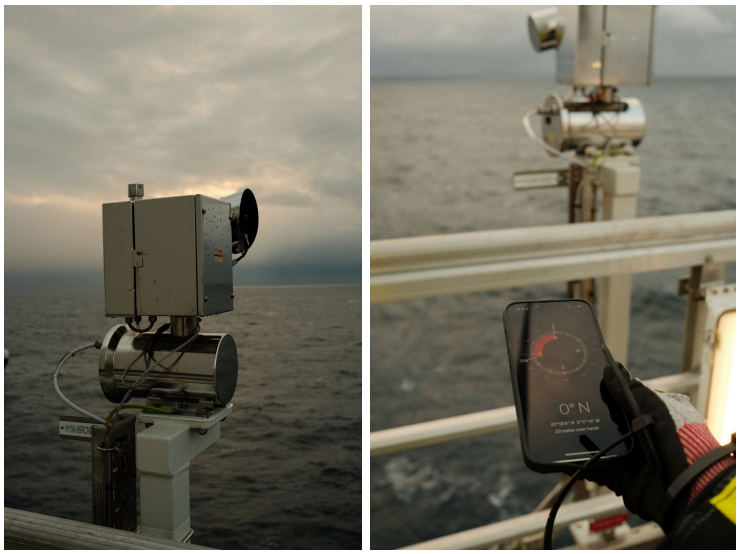

Figure 9: The CCTV camera mounted on turbine HY06. Pictures taken by an Equinor operations engineer 7 March 2024.

Figure 10: Two positions of the camera at turbine HY06: The HSE-position (left) and the bird monitoring position (right).

The cameras were programmed by Equinor's staff so that each camera returns to the bird monitoring position whenever it is not being used for HSE purposes. Figure 11 illustrates the fixed bird monitoring position of each camera.

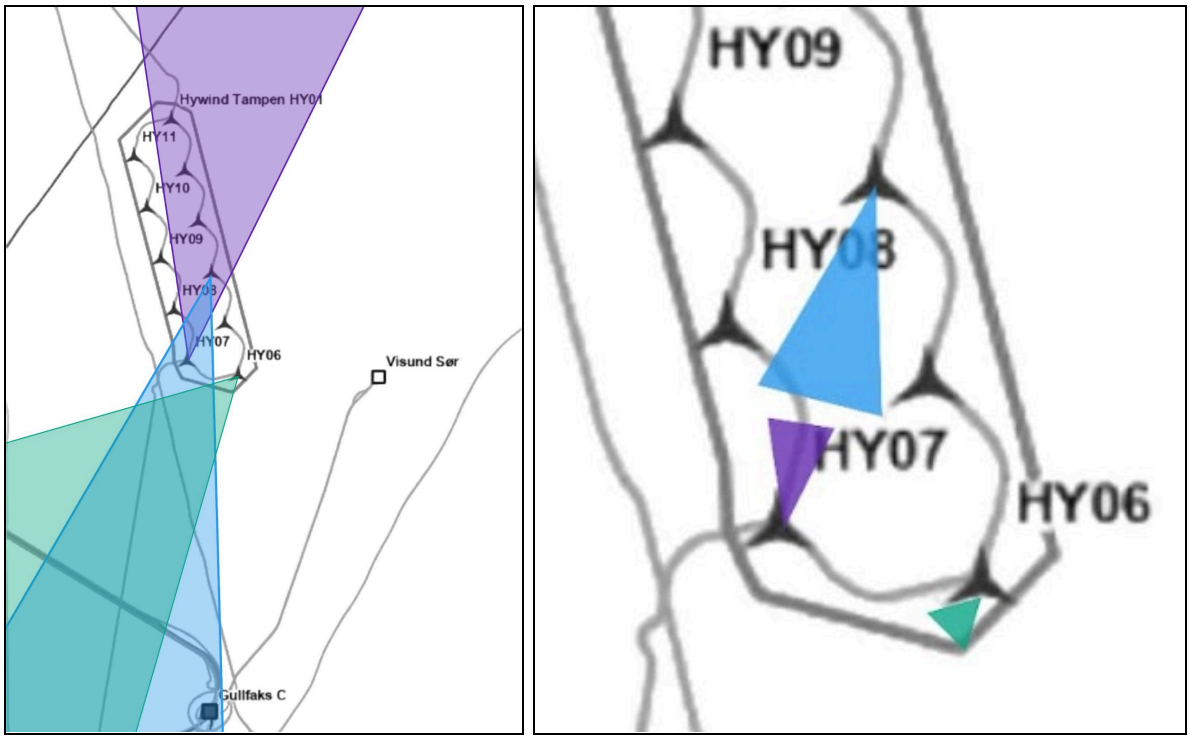

Figure 11: A representation of the camera orientations for the bird monitoring positions (left). The illustration is north/south oriented, with the Gullfaks oil field towards south. The detection range per viewpoint of a bird of 1 m wingspan is indicated by the coloured areas in the rightmost illustration.

The three vantage points selected for this pilot were on turbines HY04, HY06 and HY07, and the cameras were identified with numbers 8, 13, and 16 respectively. For the rest of this report, these will be referred to from north to south as viewpoint A (turbine HY04, camera 8), viewpoint B (turbine HY07, camera 16) and viewpoint C (turbine HY06, camera 13).

Viewpoint A

Facing south/south-west, from the vantage point of turbine HY04, the field of view is towards the middle of the wind farm, as seen in Figure 12. Turbine HY07 – viewpoint B – is in the middle of the field of view as seen in Figure 13. The distance between HY04 and HY07 is approximately 2.6 kilometres.

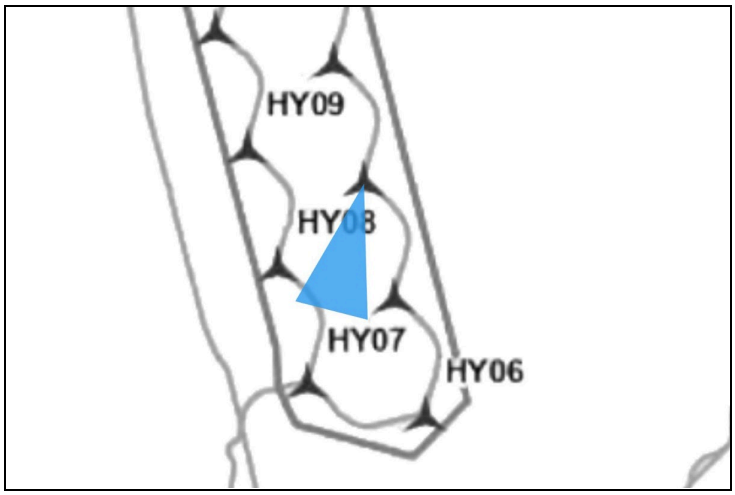

Figure 12: The camera orientation and position of viewpoint A, indicated in blue. The blue area illustrates the detection range of a bird with a 1 m wingspan.

Figure 13: The track of a Great Black-backed Gull captured from viewpoint A. Turbine HY07 (viewpoint B) is visible in the middle of the field of view. An oil platform in the Gullfaks field is visible behind HY07, a second is visible towards the leftmost side of the horizon.

Viewpoint B

As seen in Figure 14, the camera is facing north/north-east. From the vantage point of turbine HY07, the field of view is almost directly opposite viewpoint A and towards the middle of the wind farm.

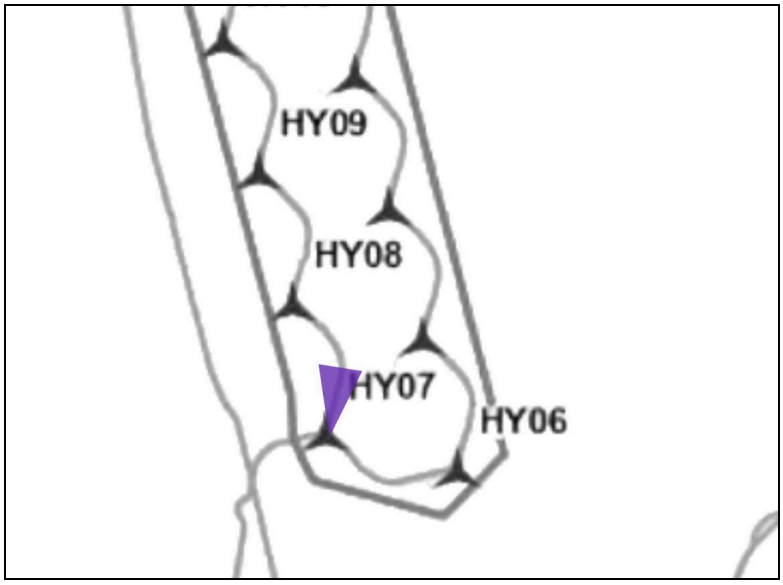

Figure 14: The camera orientation and position of viewpoint B, indicated in purple. The purple area illustrates the detection range of a bird of 1 m wingspan.

Figure 15: The track of a great black-backed gull (red dots) passing through the wind farm, as seen from viewpoint B. Turbines HY01 - HY04 are visible from left to right in the field of view.

Viewpoint C

As seen in Figure 16, the camera faces south-west, the same direction as viewpoint A. From the vantage point of turbine HY06, the field of view is the edge of the wind farm towards the open sea, as seen in Figure 17 .

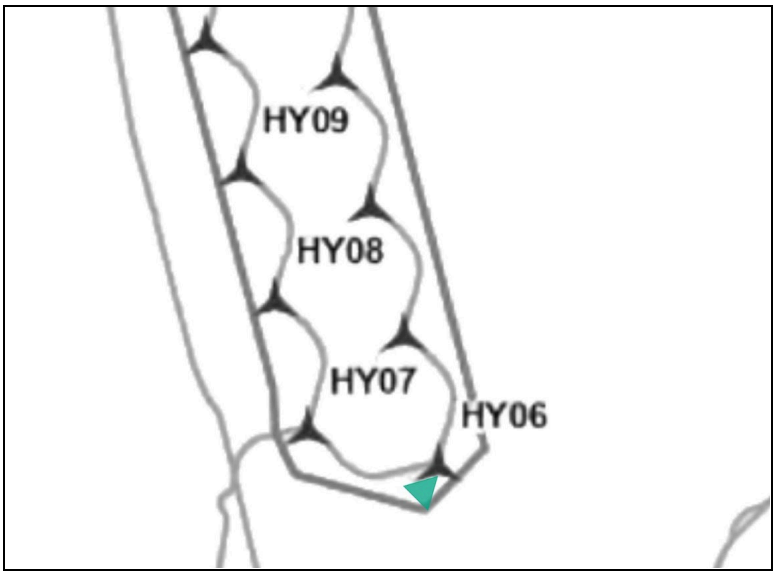

Figure 16: The camera orientation and position of viewpoint C, in green. The green area illustrates the detection range of a bird with a 1 m wingspan.

Figure 17: The track of a barn swallow captured from viewpoint C. Two oil platforms at the Gullfaks oil field are visible in the leftmost horizon.

Viewpoint properties

The cameras at each of the three viewpoints have different orientations and settings, as listed in Table 2. As discussed in the chapter *Surveillance cameras as sensors,* the camera properties, settings and orientation determine the maximum bird detection distance (range) and height

(altitude). On Hywind Tampen, the cameras have focal lengths ranging from 36mm on viewpoint A to just 4.5mm on viewpoint C. As stated in *The Hernis CCTV Cameras* chapter, the lowest possible focal length is 4.5mm, while the highest is 135mm. The difference in focal lengths translates directly to substantial differences in estimated maximum detection distance and height for each of the viewpoints. For a bird with a 1m wingspan, the estimated detection range for viewpoint A is ~1,500 m and for viewpoint C it is ~200 m.

	Viewpoint A	Viewpoint B	Viewpoint C
Turbine	HY04	HY07	HY06
Camera Height above sea	19 m	19 m	19 m
View Direction	S/W	N/E	S/W
Camera pitch	1.5°	5°	11°
View orientation inwards or outwards from wind farm	Inwards	Inwards	Outwards
Focal length	36 mm	15 mm	4.5 mm
Estimated detection distance for bird of 1m wingspan	~1,500 m	~ 650 m	~ 200 m
Estimated detection height for bird of 1m wingspan	~130 m	~140 m	~100 m
Estimated detection space for bird of 1m wingspan	~12,300,000 m^3	~5,000,000 m^3	~1,300,000 m^3

Table 2: Parameters of the camera settings, ranges and orientations per viewpoint. The differences in focal lengths explains the notable differences in estimated detection distances for each viewpoint.

Figure 18 gives a schematic representation of how the field of view changes according to the focal length of the cameras for each viewpoint. A high focal length (“high zoom”) optimises for a large detection distance, allowing for distant birds to be detected, but with the tradeoff of less monitored space in the vicinity of the camera. A low focal length (“low zoom”) yields lower detection distance, but with the benefit of a larger monitored space in the vicinity of the camera, allowing for more close-up birds to be detected.

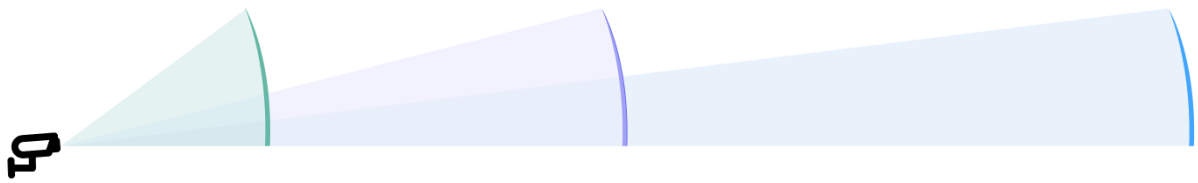

Figure 18: An illustration of the relative detection ranges for each viewpoint, determined by the focal length of the cameras. Blue represents viewpoint A with an estimated detection range of ~1,500 m for a bird of 1 m wingspan, purple represents viewpoint B, and green represents viewpoint C with the corresponding detection range of ~200 m.

Weather data

Weather data has been retrieved from *The Norwegian Centre for Climate Services: Observations and weather statistics* (n.d.), from the meteorological station located at Gullfaks C, approximately 10 km south of the Hywind Tampen wind farm. The station is 80 metres above sea level.

This source provides a granular time series of wind direction, wind speed, air and sea temperature, visibility, and cloud cover, but it does not give data on precipitation. Wind is defined in terms of the direction the wind is coming from.

Data transfer and storage

As illustrated in Figure 19, the data transfer from the cameras to the Spoor cloud storage was configured and controlled by Equinor. Equinor filtered the data and only transferred videos when the cameras were in bird monitoring position. One of the reasons for this was to limit data transmission and not transfer video that would not be useful for Spoor's analysis. Another reason was to protect any personal identifiable information that could have been captured during the HSE monitoring of human operations.

The data was in the format of .mp4 video segments of varying duration below 6 minutes, and was transferred in batches from Equinor to Spoor's AWS cloud storage. When receiving a batch of data, Spoor filtered out video files that did not have sufficient daylight. Videos with sufficient daylight were then automatically analysed by the AI system. Spoor AI deploys a collection of algorithms and strategies that allows for efficient detection and tracking.

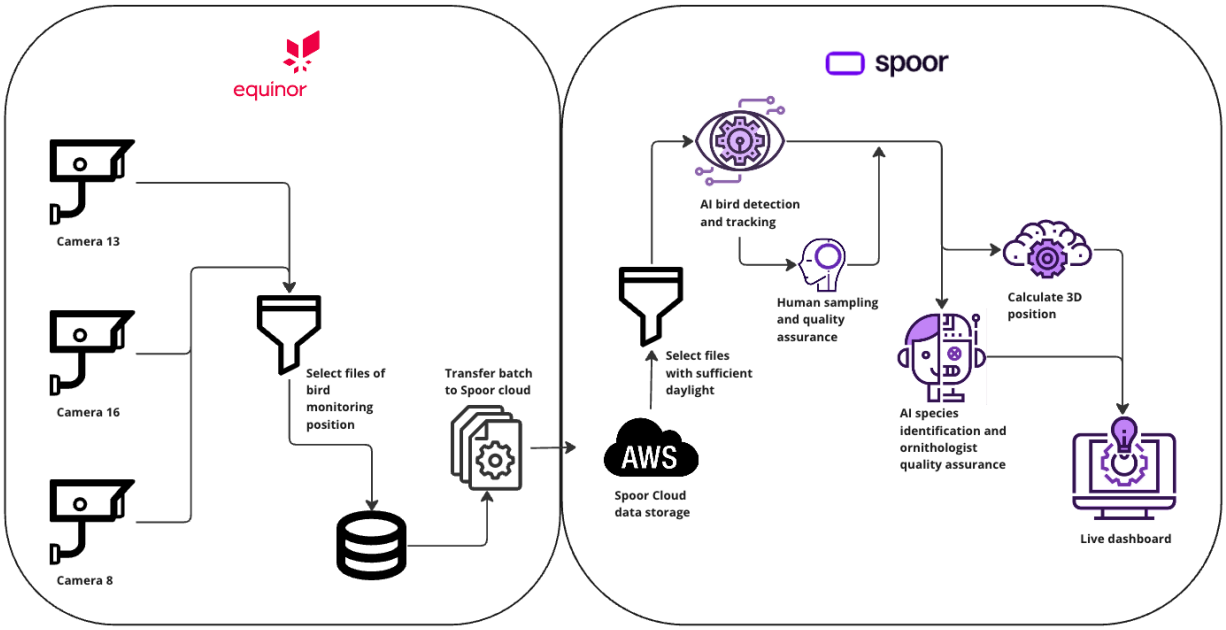

Figure 19: The data flow, storage and processing from data capture (left) to result visualisation (right). Equinor controlled the first part of the pipeline from the data capture to the batch transfer of data to Spoor's cloud.

After bird detection and tracking, species were identified with an ornithologist's quality assurance, and the system subsequently calculated the position of the bird. Results were displayed on a continuous basis in a client-facing dashboard.

Results

Measurement periods

The data capture and analysis was planned for 1 year, originally from November 2022 to November 2023. Due to delays related to installation of turbines and cameras, data protection and data flow, the first data captured from viewpoint C was 9th May 2023. Data capture from viewpoint A and B started 20th and 23rd June 2023. The last data capture was 6th February 2024, yielding a total observation period of 274 days. 195 of these days had data of sufficient quality to allow for Spoor AI analysis, while 79 days had no data transfer, or images which were too dark to be processed.

	Overall	Viewpoint A	Viewpoint B	Viewpoint C
Data capture start	9th May 2023	20th June 2023	23rd June 2023	9th May 2023
Data capture end	6th February 2024	6th February 2024	6th February 2024	6th February 2024
Number of days in the measurement period	274	232	229	274
Number of days with data of sufficient quality for Spoor AI analysis	195	147	170	174
Number of days with no data or insufficient quality	79	85	59	100

Table 3: The measurement periods across all three viewpoints, and per viewpoint.

Spoor received a total of 8.9 TB of data, (approximately 6,000 hours), as illustrated by the light green columns in Figure 20. Note that in the first weeks there were a number of changes when configuring the data stream, and the incoming raw data is therefore not completely represented in Figure 20. From mid-June, data was recorded for 19 hours per day, starting at 05:00 and ending at midnight. At the onset of winter, a lower amount of the received data was usable/could be analysed by Spoor due to lack of daylight. As seen in Figure 20, around two thirds of the transmitted videos were too dark to be analysed in November and the beginning of December 2023.

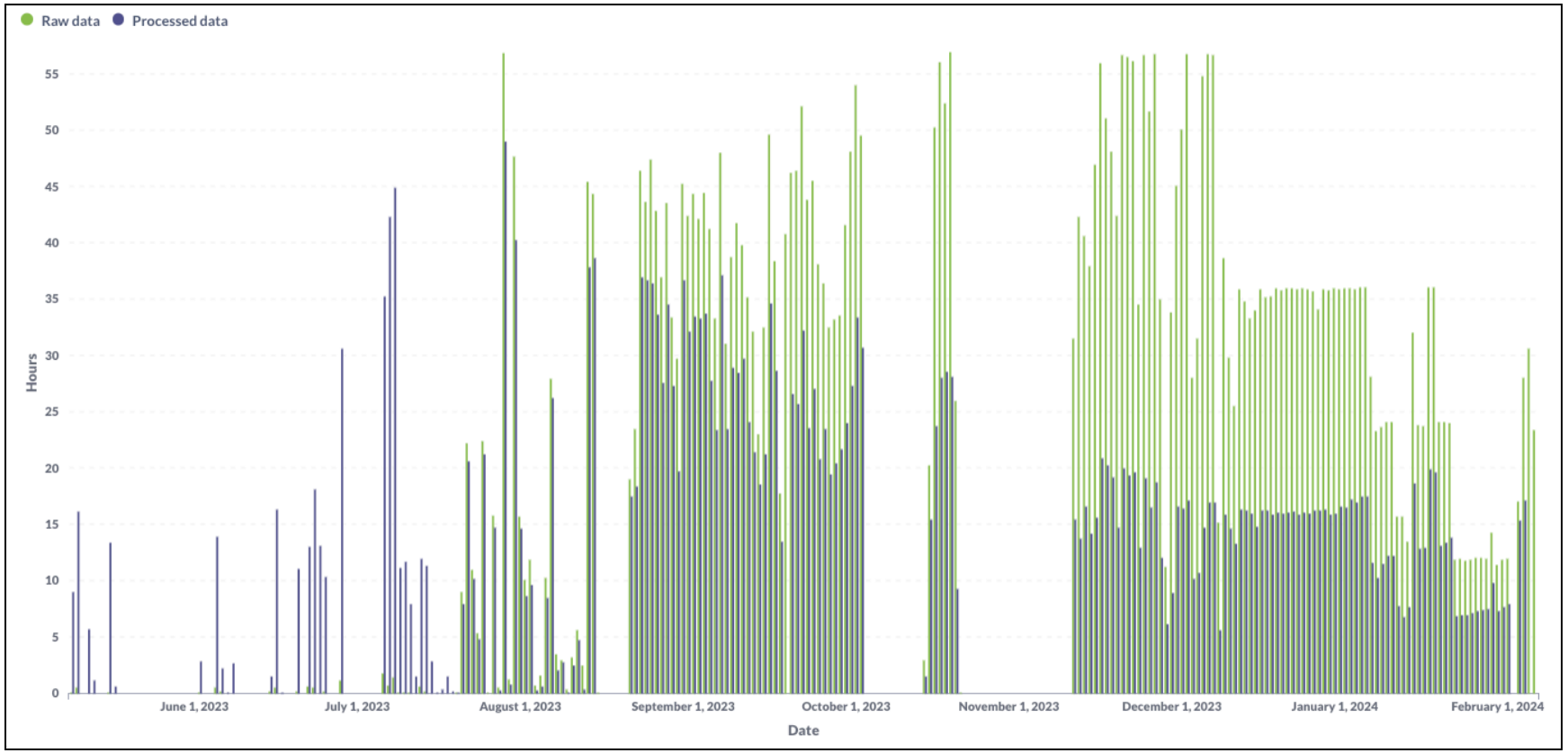

Figure 20: A representation of hours of raw video data transmitted (green) and the analysed data that were subject to AI bird detection (blue), across all 3 viewpoints. The initial tracking of the raw data from May until mid-July is not completely represented in this graph.

In mid-December 2023, Equinor reduced the data recording by several hours, as seen by the drop in the light green graph in Figure 20. It is also clear from this figure that no data were transferred for several days in October and in November. This is likely due to a breakdown of Equinor servers.

A total of 3,202 hours of video were analysed by Spoor AI; 46 hours during spring, 488 hours during summer, 1,468 hours during autumn and 1,200 hours during winter.

The observation periods varied across the three viewpoints, as illustrated in Figure 21.

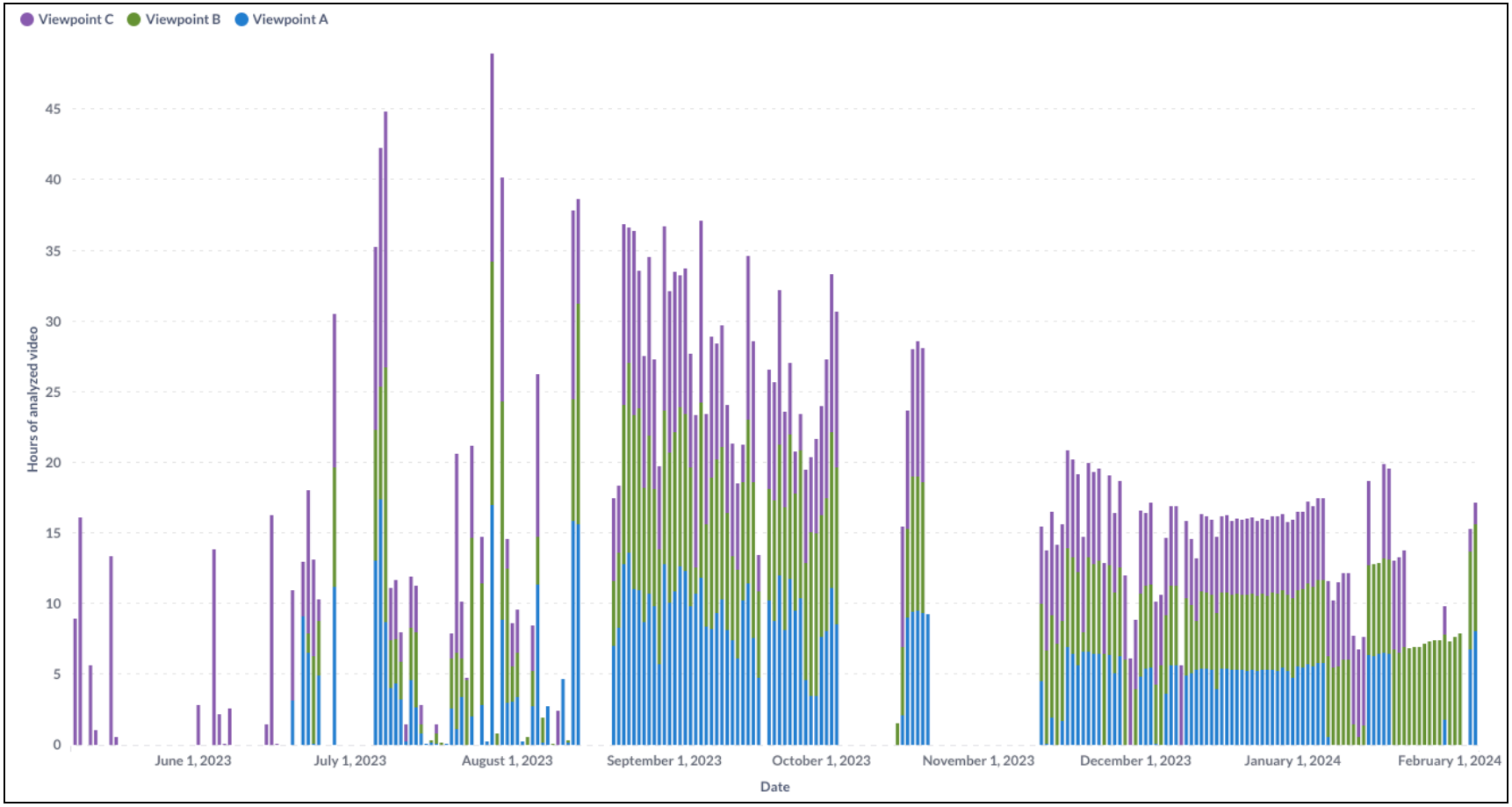

Figure 21: The number of hours of video that were analysed by Spoor AI for viewpoint A (blue), B (green) and C (purple).

The 3,202 hours of analysed video were distributed across the viewpoints in the following way:

- Viewpoint A: 947 hours
- Viewpoint B: 1,127 hours
- Viewpoint C: 1,128 hou

Data quality

Reduction of frame rate experiment

The default setting on the video stream was 30 frames per second (FPS). In order to experiment with a lower file size, the frame rate was reduced to 1 FPS between 31 January and 10 February 2024. The result of an initial analysis of 50 videos was that the current Spoor algorithm needed configuration and training for the bird detection and tracking to work, which was outside of the scope for this project.

Video file quality

Spoor analysed approximately 58,600 video files from the three viewpoints. Each file had the timestamps of video start and video end included in its filename, and the video duration of each file was found by reading the file name.

Nearly 60% of the files were of 5 minutes duration, the rest were of lower duration. The distribution of duration is shown in Figure 22. 1,579 files (2%) were registered as 0 seconds of duration. Videos of 0 seconds duration are distributed across the measurement period, with a peak on 23 August 2023 with a total of 102 video files with 0 duration.

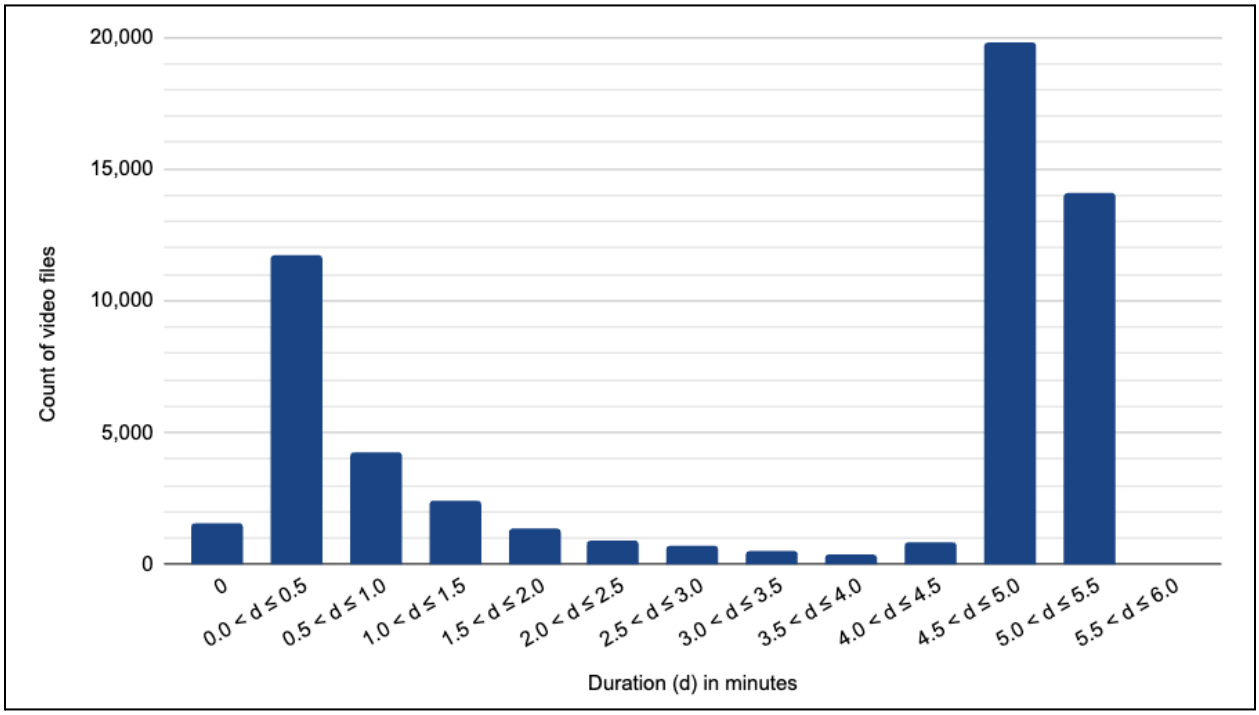

Figure 22: The count of video files that were analysed by Spoor AI, per video duration (in minutes).

Figure 23 shows files that appeared with a duration of over 0.2 hours. However, upon inspection of the file *Camera16Stream1_2023-09-13T10-44-30_2023-09-13T11-39-32*, which appeared to have a duration of 0.92 hours, the duration was found to be only 40 seconds.

video_name_id	Video duration (hours)
Camera13Stream1_2023-06-16T09-45-31_2023-06-16T16-57-10	7.19
Camera16Stream1_2023-08-25T10-18-37_2023-08-25T12-00-30	1.7
Camera16Stream1_2023-06-25T08-37-58_2023-06-25T09-36-59	0.98
Camera16Stream1_2023-09-13T10-44-30_2023-09-13T11-39-32	0.92
Camera8Stream1_2023-06-25T08-43-50_2023-06-25T09-36-54	0.88
Camera8Stream1_2023-08-30T10-05-06_2023-08-30T10-54-18	0.82
Camera16Stream1_2023-09-06T15-33-07_2023-09-06T16-00-52	0.46
Camera8Stream1_2023-08-31T07-44-08_2023-08-31T08-00-50	0.28

Figure 23: 8 files appeared by the filename to have a duration of more than 0.2 hours.

Water droplets obstructing the field of view

On 63 days out of the 195 recording days there were no bird observations recorded across any of the three viewpoints (see Figure 31). A small manual sampling of videos from days of no bird detections revealed several examples of water droplets obstructing the view. Figure 24 shows an example of the field of view obstructed by water droplets. In this example, the obstruction was not too severe and Spoor AI still detected and tracked the gull despite the effect of water droplets on the lens.

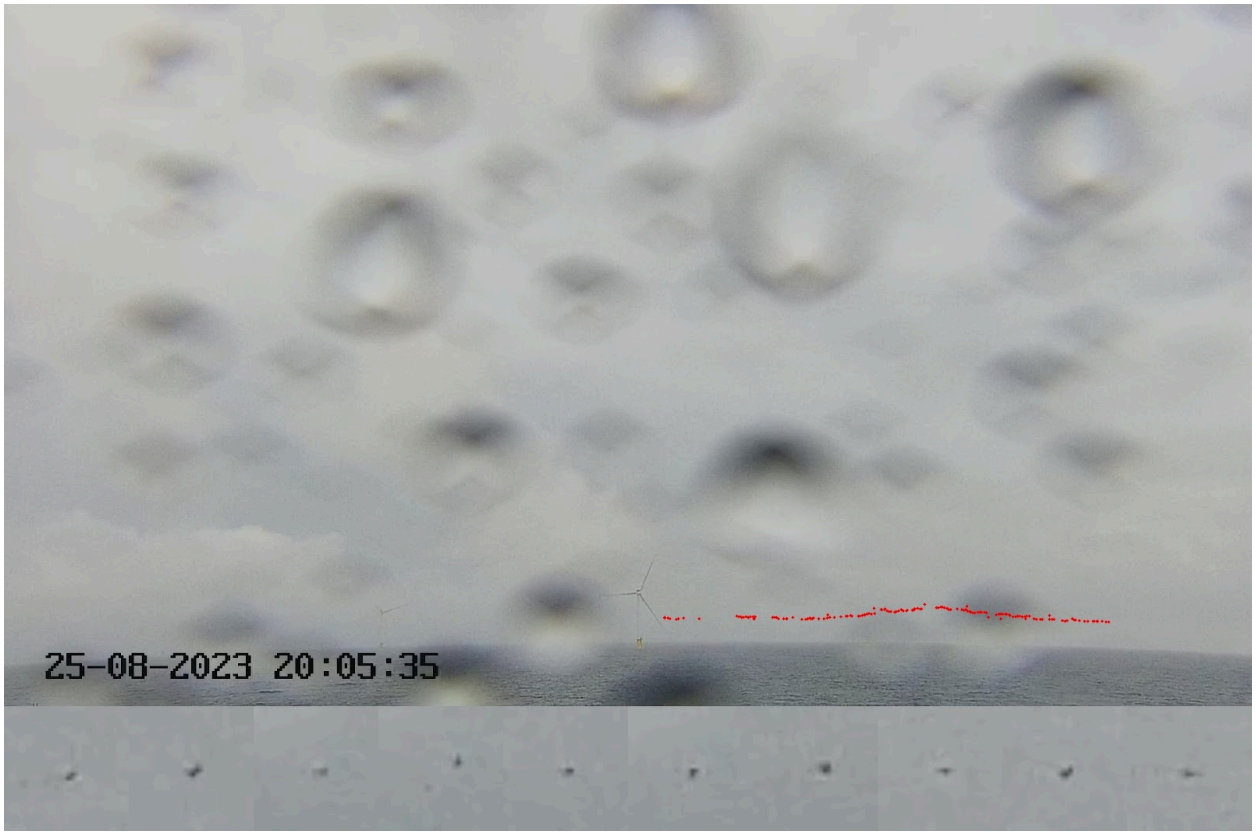

Figure 24: The track (in red) of a gull captured at viewpoint B despite water droplets obstructing the field of view. Snapshots of the bird are displayed at the bottom of the image.

In several examples, the same pattern of water droplets persisted for several minutes. In Figure 25, the same droplets on the lens at 08:07:26 are still there at 08:12:30, 5 minutes later.

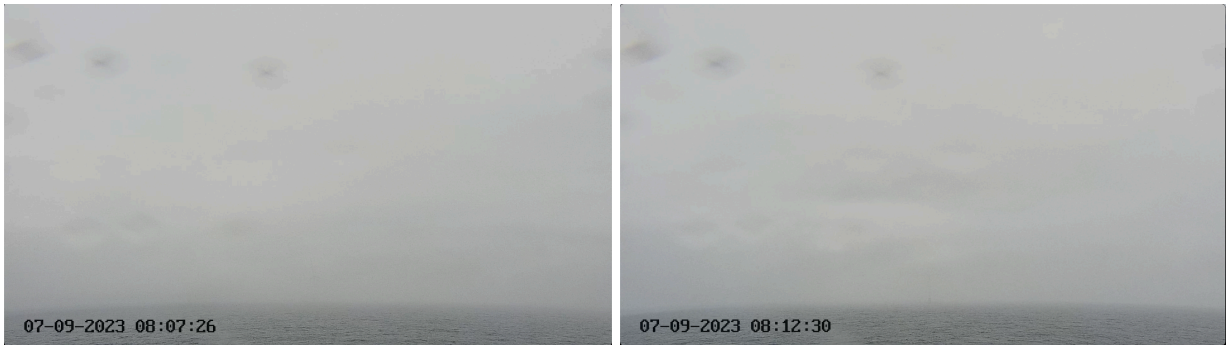

Figure 25: Pattern of water droplets on the lens (left) are still visible after 5 minutes (right). Pictures from viewpoint B.

Sun flare of south-facing cameras

Both viewpoints A and C are oriented southwards, and can be subject to sun flare and other effects due to direct sunlight. Figure 26 shows two examples of effects caused by the sun for

each of these viewpoints.

Figure 26: Two examples of sun rays striking the camera lens on viewpoint A (left) and viewpoint C (right). Notice the track of a black-backed gull visualised in red in the right-hand image.

Effects on field of view by a moving foundation

Changes in the field of view, caused by the fact that cameras are mounted on floating turbines which move according to swells, waves and wind.

Figure 27: 15 seconds distinguish the view of the left and right image. The change of view is evident by the vertical position of the turbine in the field of view. Viewpoint A. Caused by movements of the floating turbine.

Figure 28: One day distinguish the views of the left and right image. Two Great Black-backed Gulls passing through the field of view of viewpoint B.

Bird observations at Hywind Tampen

Spoor AI counted a total of 1,455 bird observations across the three viewpoints, distributed on 195 days across the four seasons: 12 observations during spring, 236 during summer, 719 during autumn and 488 during winter. In Figure 29, counts of bird detections are colour-coded to reflect the seasons.

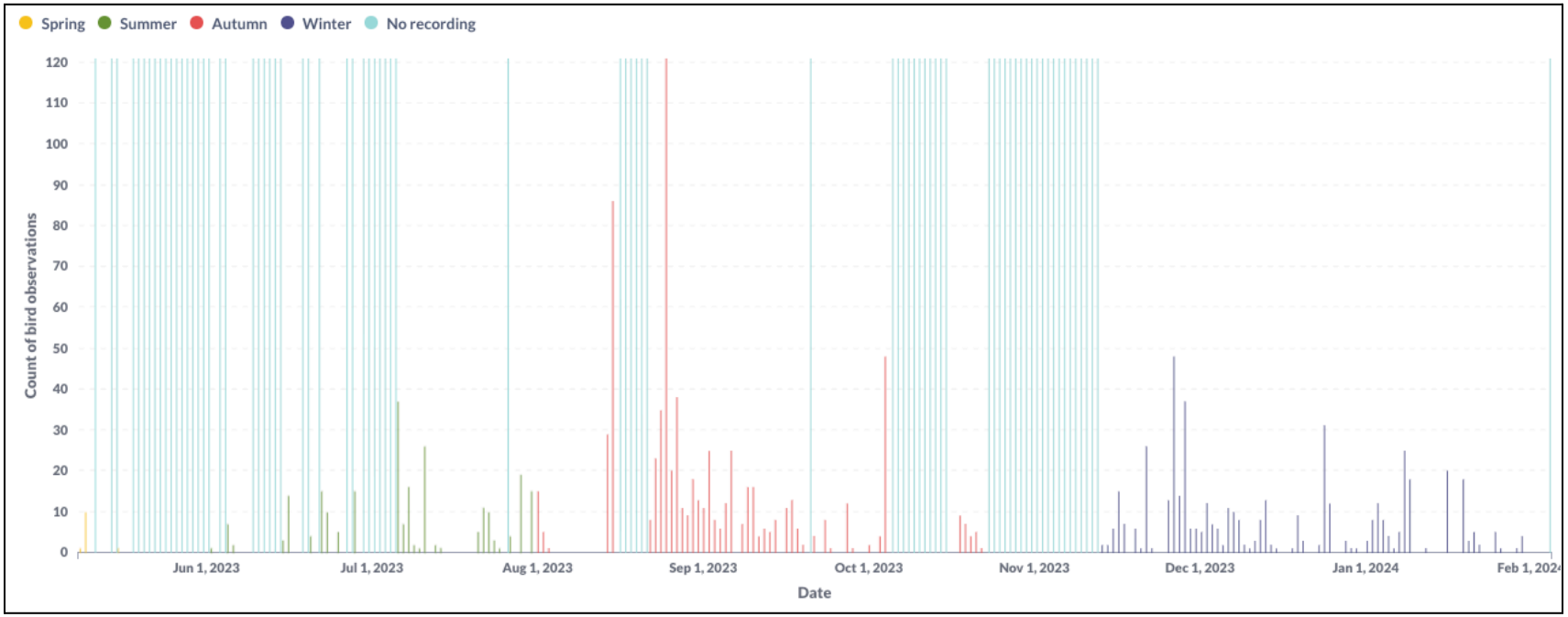

Figure 29: The daily count of bird observations across all three viewpoints. Yellow columns represent observations during spring, green represent summer, red represents autumn and blue represents observations during winter. Days of no analysed data are indicated in light blue.

The observation rate can be normalised as the number of bird observations, divided by the number of analysed hours. The unit can be per day, season, year, or other. This unit is useful as it accounts for the difference in the number of analysed hours. The seasonal variations in observation rate for the three viewpoints combined are listed in Table 4, and the daily observation rates are visualised in Figure 30.

	Spring May 2023	Summer June-July 2023	Autumn August-October 2023	Winter November 2023 - February 2024
Analysed hours Videos of sufficient quality for Spoor analysis	46 h	488 h	1,468 h	1,200 h
Count of bird observations	12	236	719	488
Observation rate Observations/hour	0.26	0.48	0.49	0.41

Table 4: The number of analysed hours, count of bird observation and the derived observation rate per season, across the three viewpoints.

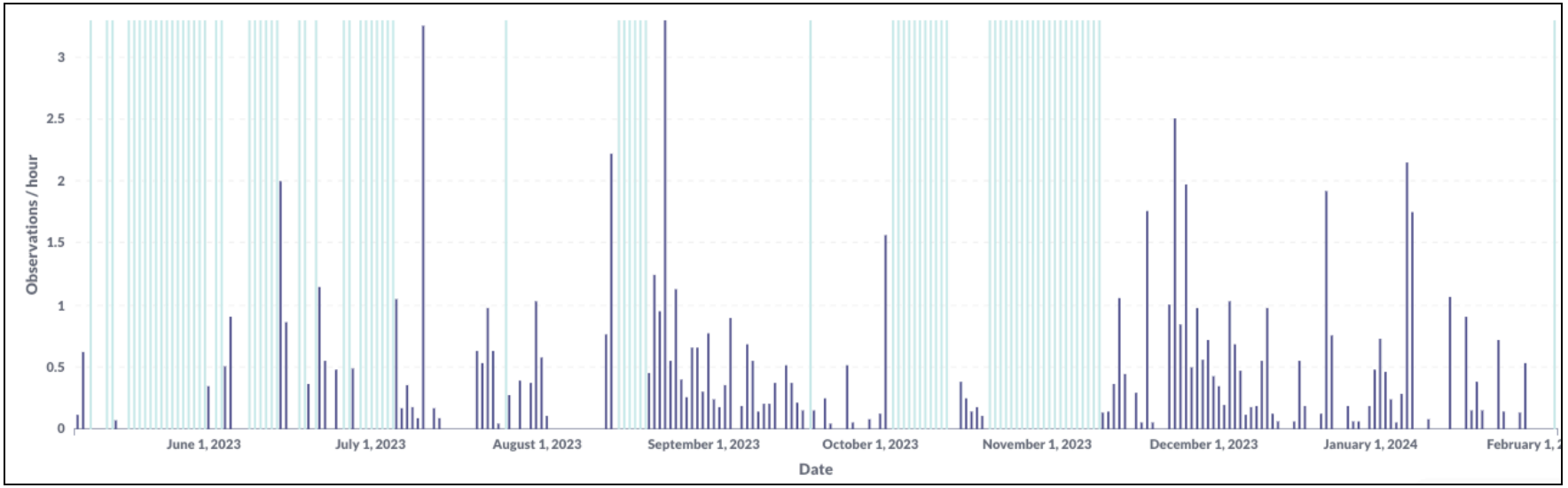

Figure 30: The daily observation rates (observations/analysed hours/day) for the three viewpoints. Days where data was either of too low quality to be analysed, or no data were received, are indicated in light blue.

According to Figure 30, the days with the highest observation rates were 25 August 2023 with an average of 3.3 bird observations per hour, followed by 11 July 2023 with 3.26 observations per hour, and 26 November 2023 with 2.51 observations per hour.

From another perspective, the purple columns in Figure 31 indicate days with no bird observations despite having observation time. 63 days out of 195 observation days had no bird observations, most notably 25 September 2023 and 2 October 2023 which each had 27 hours of analysed data, and 7 August 2023 with 26 hours of analysed data. 35 of the 63 days of no bird observations had less than 10 hours of analysed data across all three viewpoints.

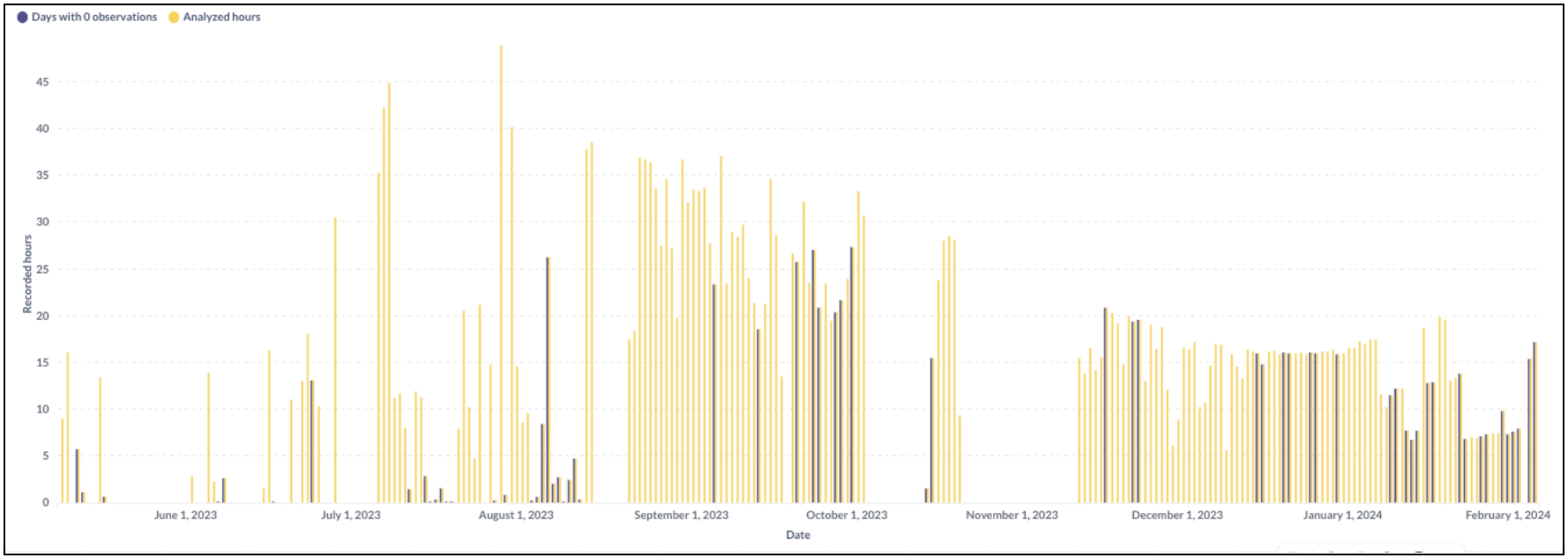

Figure 31: Days without observations (purple) and days with bird observations (yellow).

Species

All of the 1,455 bird observations have been subject to taxonomic classification with the following results:

- 724 (50%) could be classified to species level
- 1,293 (89%) could be classified to family level
- 1,309 (90%) could be classified to order level

This means only 10% of the observations could be classified to class level “bird”.

As seen in Table 5, birds within six different orders and of nine different species were identified. The majority are seabirds, and 1,234 (85%) of the identified birds are gulls. The black-legged kittiwake has Norwegian red list status *endangered*, and the European herring gull has status *vulnerable,* according to *Artsdatabanken: Norsk rødliste for arter 2021 (2021)*. The other species do not have a protected status.

Taxonomy (order, family, species)	Bird count family or order level	Bird count species level	Red list status*
Charadriiformes; Shorebirds			-
- Gulls and Terns	564		-
Great Black-backed Gull (*Larus marinus*)		666	LC
European Herring Gull (*Larus argentatus*)		1	VU
Black-legged Kittiwake (*Rissa tridactyla*)		3	EN
- Skuas and Jaegers			-
Great Skua (*Stercorarius skua*)		1	LC
- Sandpipers and Allies	2		
Suliformes			-
- Cormorants and Shags	5		-
- Boobies and Gannets			-
Northern Gannet (*Morus bassanus*)		30	LC
Piciformes			-
- Woodpeckers			-
Great Spotted Woodpecker (*Dendrocopos major*)		1	LC
Procellariiformes			-
- Shearwaters and Petrels			-
Northern Fulmar (*Fulmarus glacialis*)		17	LC
Passeriformes; Passerines	13		
- Swallows			-
Barn Swallow (*Hirundo rustica*)		4	LC
- Wagtails and Pipits			-
White Wagtail (*Motacilla alba*)		1	LC
Accipitriformes; Raptors	1		-

Table 5: The count of observed birds per order, family and species level.
**LC = Least Concern, VU = Vulnerable, EN=Endangered*

Figures 32-36 shows examples of identified birds and their flight tracks, as they are presented in the Spoor webapp. Birds typically appear very small when a video frame is presented as an image, and 10 zoomed-in snapshots of the bird from various points along its flight track are attached at the bottom of each track image. Note that these images are made for illustrative purposes, and are not the basis for taxonomy classification. In the webapp, the full video segment is available for the viewer to play at their convenience.

Figure 32: The track of a Black-legged Kittiwake (in green dots) captured 15 August 2023 at Viewpoint B. Some of the close-up snapshots of the kittiwake have been distorted in order to fit the full bird into a square frame.

Figure 33: Two tracks of Northern Gannets captured on 6 July 2023, from viewpoint B (left) and viewpoint C (right)

Figure 34: Two tracks of Great Black-backed Gulls (in red) captured at viewpoint B, at 28 June 2023 (left) and 25 August 2023 (right).

Figure 35: The track of a Great Black-backed Gull (green) captured at viewpoint B on 22 June 2023.

Figure 36: The track (in green) of a Great Spotted Woodpecker captured at viewpoint C.

Table 6 shows the seasonal distribution of the observed birds. Five different species and families were identified during winter and summer, and three during spring. Eight different species and families (not including “gull”) were identified during autumn.

Taxonomy Species, Family, Order	Spring May 2023	Summer June-July 2023	Autumn August-October 2023	Winter November 2023 - February 2024
Sandpipers and Allies			2	
Gulls (unspecified)	2	86	216	260
Great Black-backed Gull	3	97	417	149
European Herring Gull				1
Black-legged Kittiwake			3	
Cormorants and Shags				5
Northern Gannet	2	16	1	11
Northern Fulmar			17	
Small passerine birds			11	2
Barn Swallow	4			
Great Skua		1		
Great Spotted Woodpecker			1	
Raptor		1		
White Wagtail			1	

Table 6: The seasonal distribution of identified birds across the three viewpoints.

Observations per viewpoint

Understanding bird activity and occurrences at each of the three viewpoints is useful to be able to contrast and compare the results. The 1,455 bird observations are distributed across the three viewpoints as shown in Table 7.

	Viewpoint A	Viewpoint B	Viewpoint C
Analysed hours Videos of sufficient quality for Spoor analysis	947 h	1,127 h	1,128 h
Bird observations	431 observations	467 observations	557 observations
Observation rate Observations/ analysed hour for the full measurement period	0.45 observations/hour	0.41 observations/hour	0.49 observations/hour

Table 7: The hours of analysed data, number of bird observations, and observation rate for each of the viewpoints across the full measurement period.

	Viewpoint A			Viewpoint B			Viewpoint C		
	Analysed hours	Observations	Observation rate	Analysed hours	Observations	Observation rate	Analysed hours	Observations	Observation rate
Spring May 2023	0	-	**-**	0	-	**-**	46	12	**0.26**
Summer Jun-Jul 2023	133	53	**0.40**	146	87	**0.60**	209	96	**0.46**
Autumn Aug - Oct 2023	513	245	**0.48**	497	240	**0.48**	458	234	**0.51**
Winter Nov 2023 - Feb 2024	301	133	**0.44**	484	140	**0.29**	415	215	**0.52**

Table 8: The number of analysed hours, number of bird observations and the derived seasonal observation rate per viewpoint.

Bird species

Different bird species were detected at the vantage points. Nine species and families were detected at viewpoint C, not including the unspecified gulls, and six species and families were detected for the other two viewpoints.

Taxonomy Species, Family, Order	Viewpoint A	Viewpoint B	Viewpoint C
Sandpipers and Allies	2		
Gulls (unspecified)	202	179	183
Great Black-backed Gull	150	222	294
European Herring Gull	1		
Black-legged Kittiwake		3	
Cormorants and Shags		5	
Northern Gannet	6	8	16
Northern Fulmar	8	1	1
Small passerine birds	8	2	3
Barn Swallow			4
Great Skua			1
Great Spotted Woodpecker			1
Raptor			1
White Wagtail			1

Table 9: The different species registered and the number of observations per viewpoint, for the full measurement period.

Flight directions

Viewpoint A

As seen in Figure 37, the majority of flight tracks have a direction along the S/W and N/E axis – parallel to the camera orientation. The total number of observations was 431, of which 47% (203 observations) had a direction calculated.

Figure 37: The flight directions of observed birds of viewpoint A for the full measurement period. 10% was flying towards S/W and N/E, respectively.

The seasonal variation of flight directions is shown in Figure 38. During summer, nearly 20% of observed birds were flying towards S/W, 10% towards N and N/E. During autumn, observed flight directions are quite uniformly distributed between S/W and N/E, and in winter the flight directions spread across N/E, E, S/E, S and S/W.

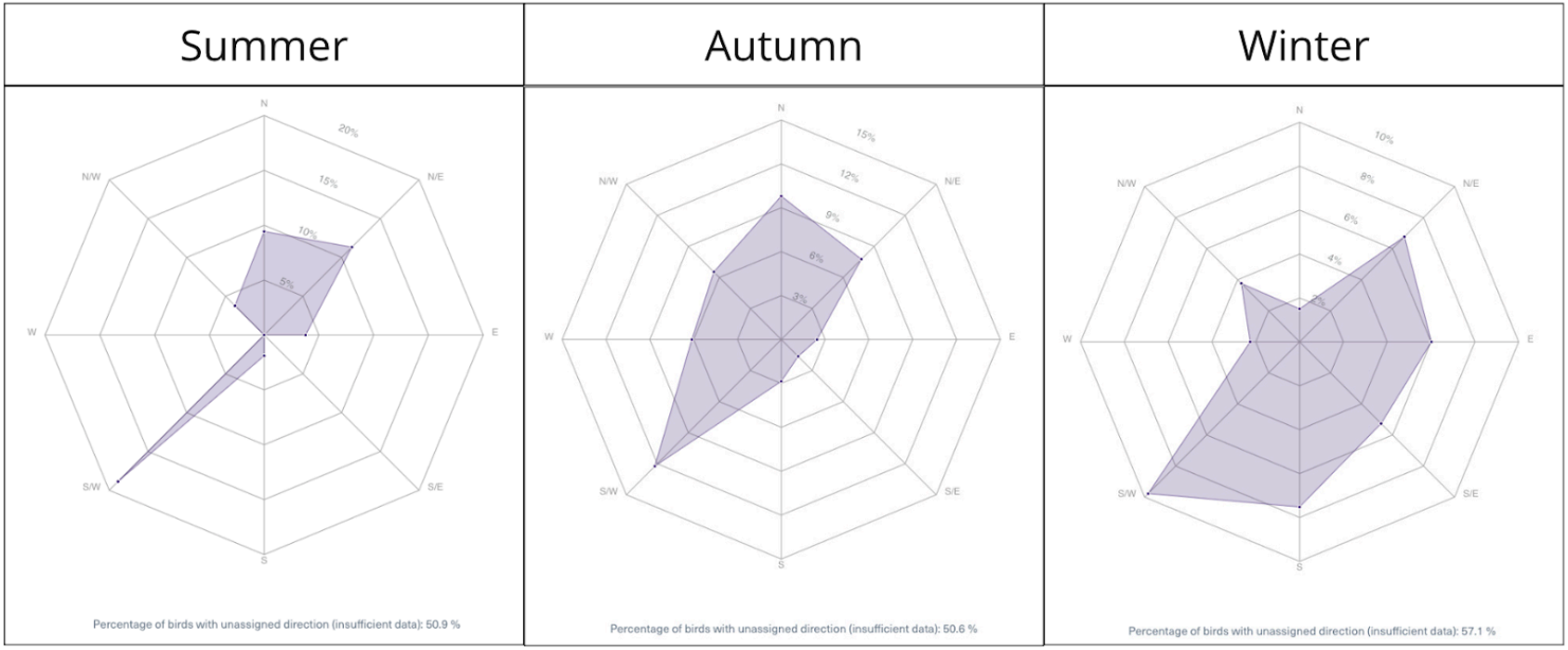

Figure 38: The seasonal differences of observed flight directions for viewpoint A. Data capture was not done during spring for this viewpoint. Note the change of value of the outer axes; 20% on the summer graph, 15% on the autumn graph and 10% on the winter graph. The percentage of observations that were not assigned a direction was 51%, 51% and 57%, respectively.

353 of the observed birds at viewpoint A were gulls, and 78 were non-gulls. Figure 39 shows the flight directions for the whole measurement period of gulls and non-gulls, respectively. 54% of gulls and 47% of non-gulls had a direction assigned.

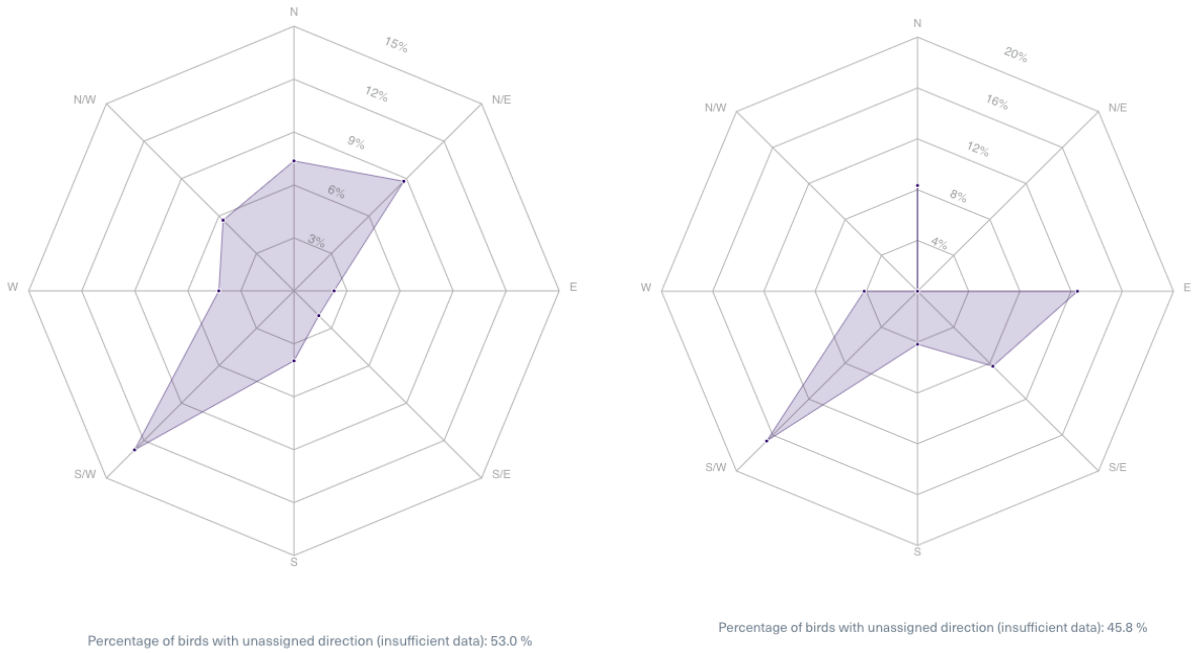

Figure 39: The cross-seasonal flight directions of gulls (left) and non-gulls (right). Both gulls and non-gulls have a dominant direction towards S/W. Gulls have a pronounced directionality along the N/E and S/W axis

Viewpoint B

As seen in Figure 40, the distribution of flight directions of the 467 track is quite uniform. 50% of the observations had a direction assigned.

Figure 40: The flight directions of observed birds from viewpoint B for the full measurement period.

The seasonal variation of flight directions are shown in Figure 41. During summer, there is an apparent spike in flight direction towards N/E (15% of all observations), but the dominating direction is S/W and W. During autumn and winter, a more uniform pattern emerges.

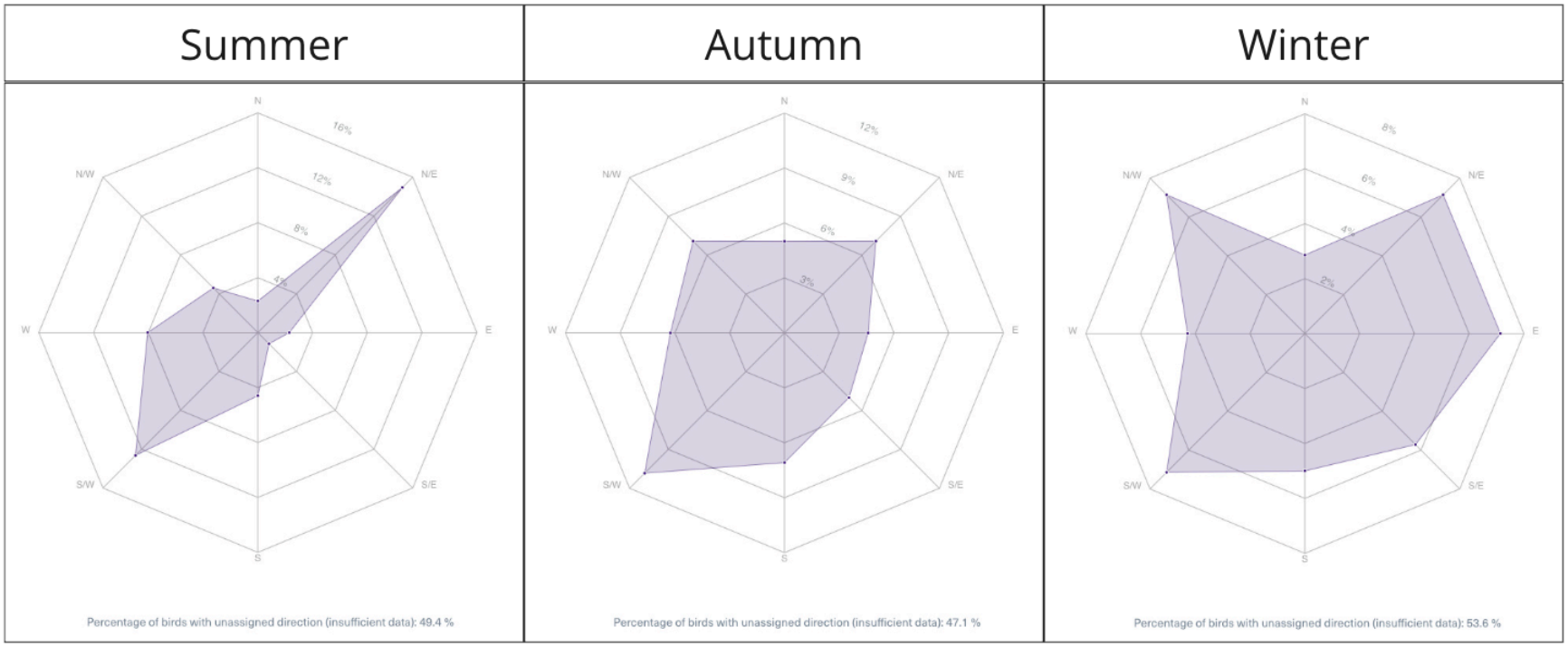

Figure 41: The seasonal differences of observed flight directions for viewpoint B. Data capture was not done during spring for this viewpoint. Note the change of value of the outer axes; 16% on the summer graph, 12% for autumn and 8% for the winter graph. The percentage of observations that were not assigned a direction was 49%, 47% and 54%, respectively

Viewpoint C

As seen in Figure 42, a majority of tracks observed from viewpoint C are directed along the N/W and S/E directions. 46% of the observed birds could not be assigned a flight direction.

Figure 42: The flight directions of observed birds of viewpoint C for the full measurement period.

As seen in Figure 43, the directional flight patterns display a similar distribution across the seasons.

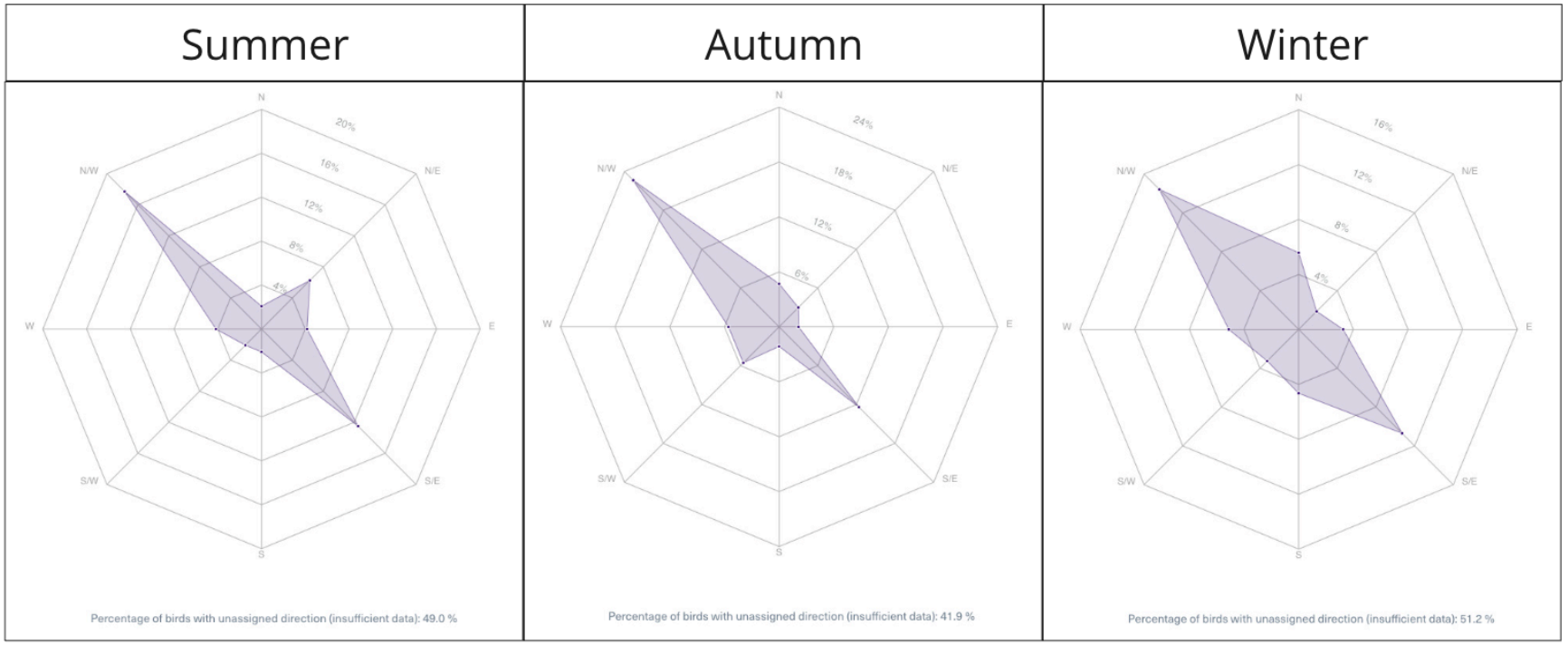

Figure 43: The seasonal flight directions for viewpoint C. Spring is not included due to low number of bird observations. Note the change of value of the outer axes; 20% on the summer graph, 24% on the autumn graph and 16% on the winter graph. The percentage of observations that were not assigned a direction was 49%, 42% and 51%, respectively.

Flight altitudes

Viewpoint A

The flight height distribution in Figure 44 is based on 54 detections across the measurement period. The observed flux peaks with 0,0013 birds/m^2 at 30 metres altitude. The estimated detection distance for viewpoint A is ~1,500 metres, as illustrated in Figure 45, and the flight heights are measured across this distance.

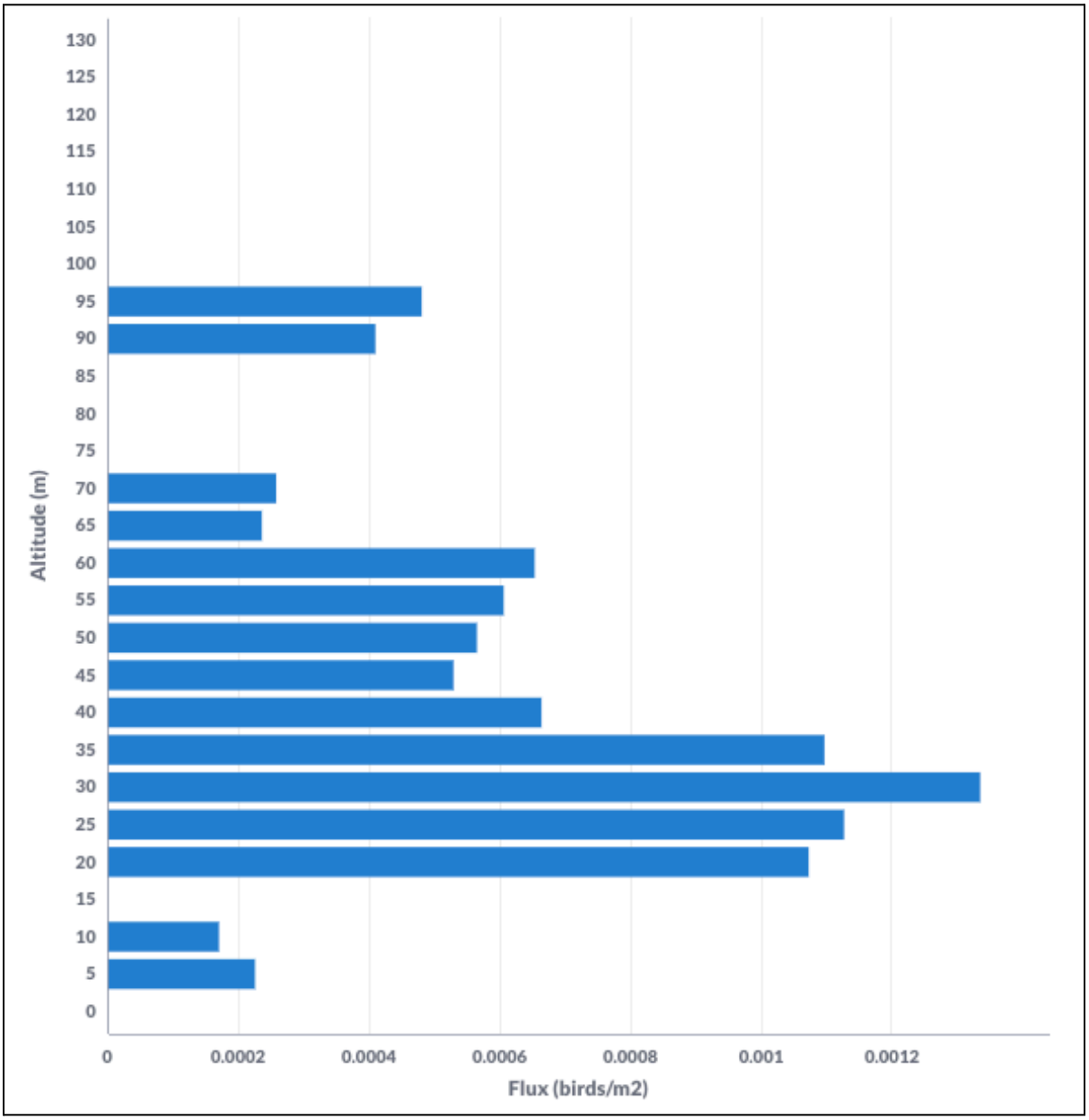

Figure 44: The flight height flux for observed birds intersecting with the middle of the field of view – see Figure 5.

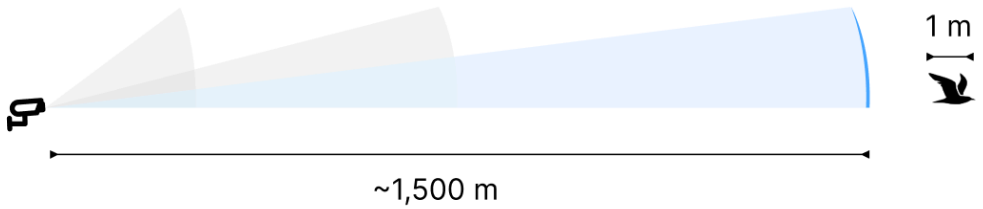

Figure 45: The estimated detection range for a bird with wingspan of 1m is ~1,500 m for viewpoint A. The flight height distribution in Figure 44 covers this range.

Viewpoint B

The flight height distribution in Figure 46 is based on 95 detections across the measurement period. At 25 metres altitude, the flux peaks at 0,006 birds/m^2

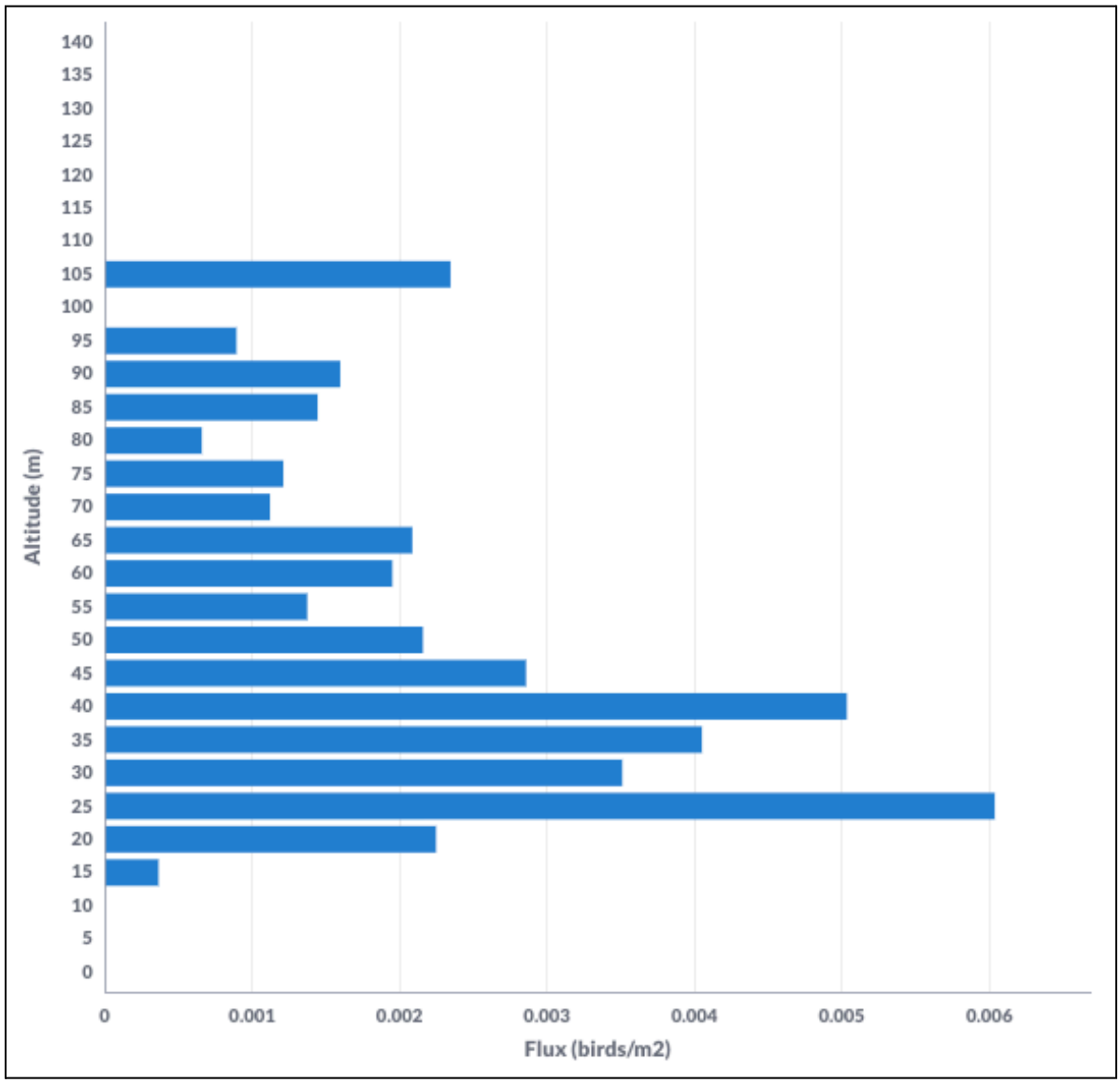

Figure 46: The flight height flux for observed birds intersecting with the middle of the field of view – see Figure 5.

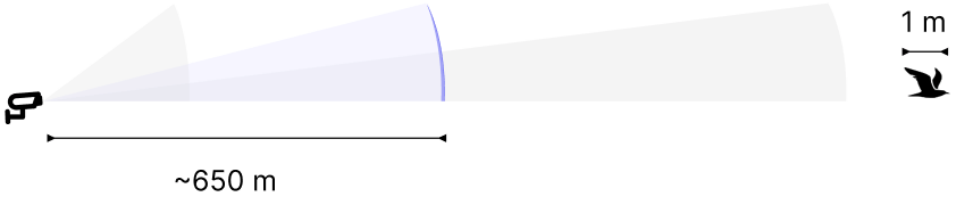

Figure 47: The estimated detection range for a bird with wingspan of 1m is ~650 m for viewpoint B. The flight height distribution in Figure 46 covers this range.

Viewpoint C

The flight height distribution in Figure 48 is based on 109 detections across the measurement period. At 20 metres altitude, the flux peaks at 0,04 birds/m^2.

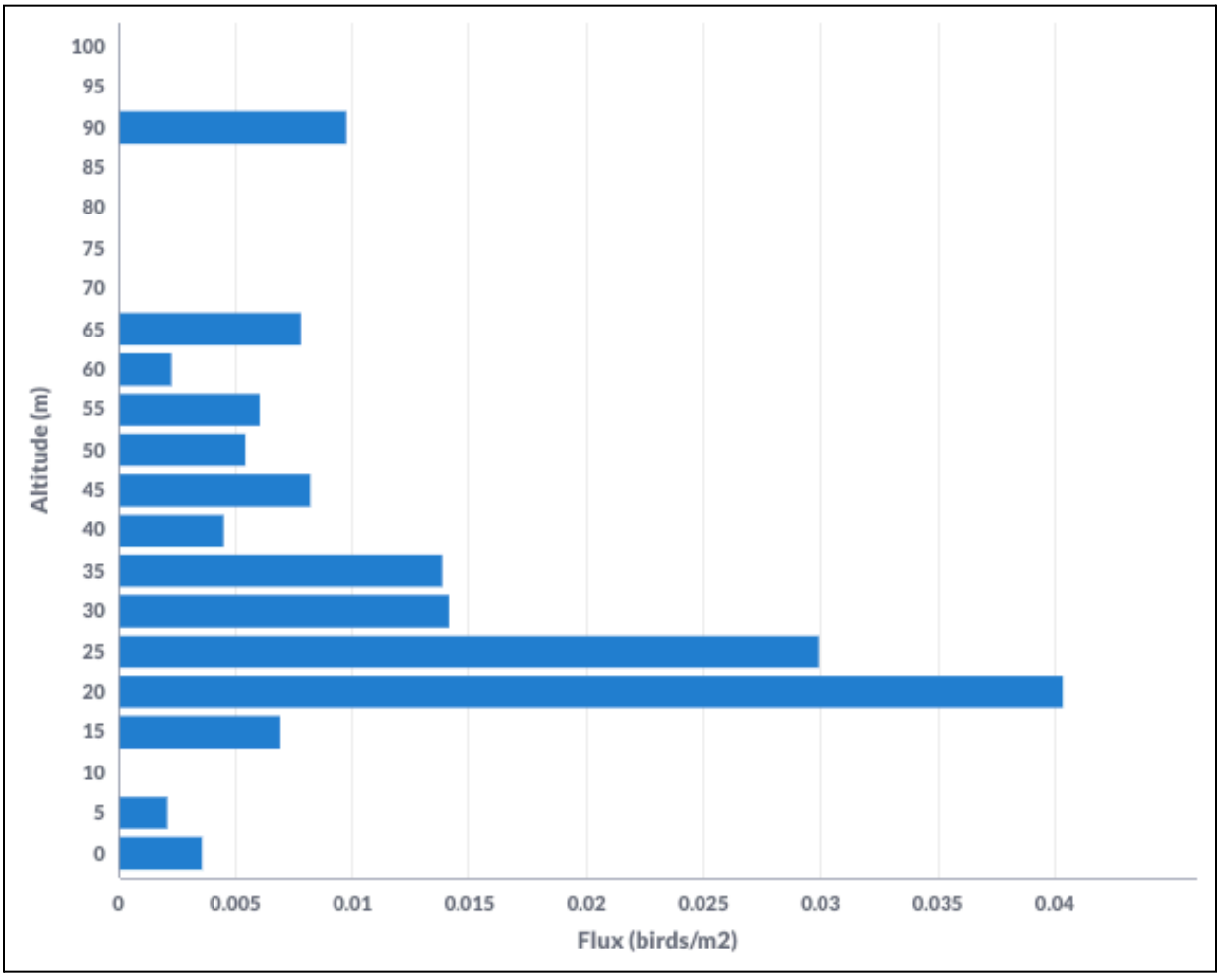

Figure 48: The flight height flux for birds intersecting with the middle of the field of view – see Figure 5.

Figure 49: The estimated detection range for a bird with wingspan of 1m is ~200 m for viewpoint C. The flight height distribution in Figure 48 covers this range.

Flight activity related to wind speed and direction

Figure 50 shows the daily bird observation rate as a function of daily average wind speed, for all days with one or more bird observations.

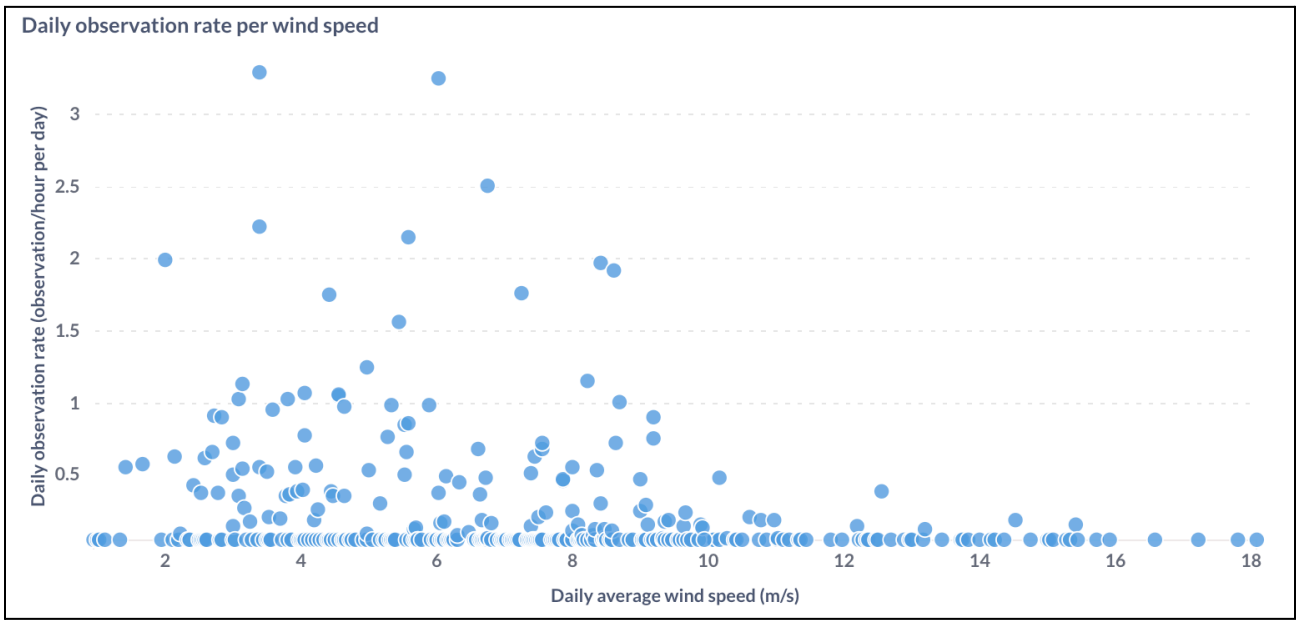

Figure 50: The daily observation rate (bird observations per number of hours analysed for each day) as a function of the wind speed.

A more granular representation is seen in Figure 51, where gull observations per hour is plotted against the wind speed per hour. Figure 52 shows the corresponding plot non-gull observations.

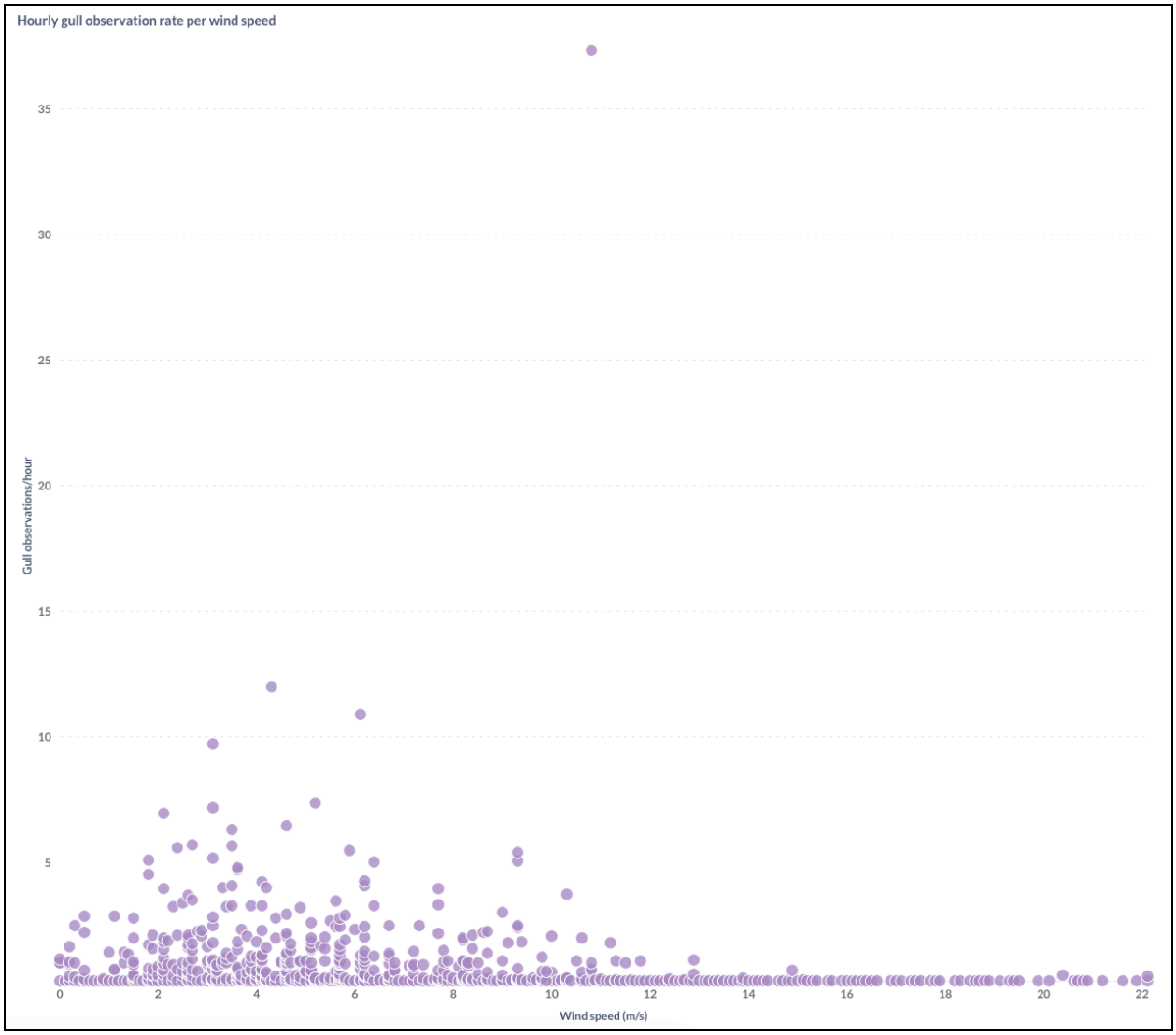

Figure 51: The hourly observation rate for gulls (gull observations per number of hours analysed for each day) as a function of the wind speed per hour.

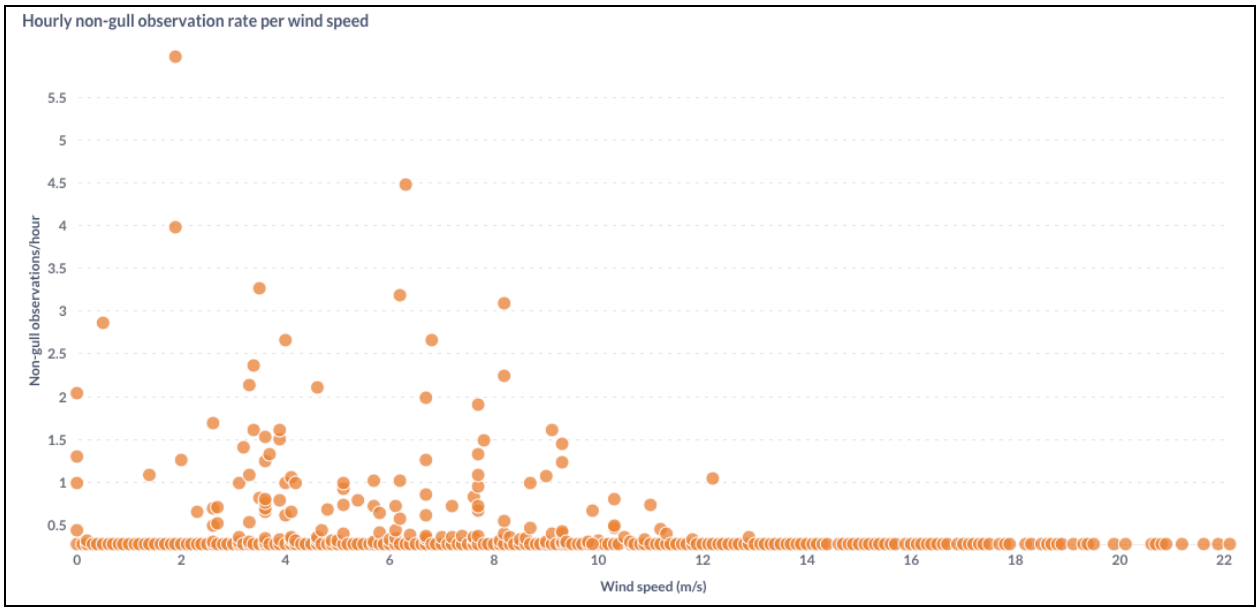

Figure 52: The hourly observation rate for non-gulls (non-gull observations per number of hours analysed for each day) as a function of the wind speed per hour.

In Table 10, the number of analysed hours, bird observations and observation rate for the full measurement period is displayed per wind direction.

	Northerly winds 315°– 45°	Easterly winds 45°– 135°	Southerly winds 135°– 225°	Westerly winds 225°– 315°
Analysed hours Videos of sufficient quality for Spoor analysis	869 h	634 h	1,026 h	673 h
Bird observations	553	280	304	326
Observation rate Observations per analysed hour for the full measurement period	0.64	0.44	0.30	0.48

Table 10: The observation rates when winds are blowing from North, East, South and West. The numbers are across all viewpoints and for the full measurement period.

Table 11 shows the seasonal distribution of the observation rate per wind direction. Higher observation rates are indicated with a darker orange colour. Three of the data points indicated with asterisks are based on a lower number of analysed hours, while the other data points are based on 100 hours or more.

Observation rate	Northerly winds 315°– 45°	Easterly winds 45°– 135°	Southerly winds 135°– 225°	Westerly winds 225°– 315°
Spring	0.28*	-	0.31**	-
Summer	0.42	0.54	0.27	0.99***
Autumn	0.97	0.40	0.25	0.48
Winter	0.44	0.44	0.39	0.35

*Table 11: The seasonal observation rate per wind direction for all three viewpoints. Darker colour indicates higher values. *25 hours of analysed data; **16 hours of analysed data, ***70h of analysed data.*

Discussion

The CCTV cameras used in this project were selected and installed without bird monitoring in mind, but rather for operational HSE monitoring. At the onset of this project, there was a great deal of uncertainty around whether it would be possible to retrieve useful bird activity data - given that the resolution of the cameras were lower compared to a standard Spoor deployment. The results, however, show that valuable data can be obtained with lower resolution CCTV cameras.

Data capture

High quality raw data is the foundation of effective monitoring and analysis and there are a number of factors which can impact data quality from offshore CCTV cameras. Without regular cleaning of the camera lenses, water droplets or other contamination on the lens can obstruct the field of view for long periods, while direct sunlight into a lens can also obstruct parts of the field of view for shorter but significant periods of time. Mechanical vibrations of the camera sensor from wind or turbine operations can also degrade the captured images. The first two effects have been observed in this pilot and will be discussed in more detail, while the latter has not been observed – which indicates a stable camera mount.

Field of view obstructed by droplets on the lens

On several occasions the patterns of droplets on the camera lense/s remained the same for several minutes at a time, indicating that the built in screen wiper system had not been used, at least not reactively in a short timeframe.

Spoor AI is able to detect and track birds during rainy weather, even when the field of view is partly obstructed. (see Figure 24). Whether a bird can be tracked despite rain/water droplets depends on how much of the image is obstructed, although we have not quantified a “cutoff” threshold because other factors such as the distance of the bird from the lens also affect this. We assume that a portion of Spoor’s AI detection and tracking has been inhibited by water droplets on the lens but again, this is not quantified. This needs to be taken into account when evaluating the results and apparent absence of birds; as in some cases an absence of bird detections can be caused by obstruction, and not the confirmed absence of birds.
We expect that the issue of droplets obstructing the view can be largely mitigated by systematically activating the wiper system when precipitation or other water condensation on the lens occurs.

Sun flare for South-facing cameras

Cameras in the Northern hemisphere that have a Southwards orientation can be subject to so called *sun flare* and other lens effects due to direct sunlight, as seen in Figure 26. These effects typically affect only parts of the field of view, and the effects will disappear once the sun angle

has changed (or the sun is hidden behind clouds etc). The sun flare can be more pronounced by impurities (contamination, salt, water droplets etc) on the lens.

Avoiding sun flare and similar effects is more complicated than removing water droplets, because the optimal solution is to orient the cameras away from the direct sunlight, or in other ways shield the lens from sun rays, which may be in conflict with the desired field of view or area of interest.

Effects on the field of view of a floating foundation

As seen in Figures 27 and 28, the field of view can change according to movements of the floating platform on which the camera is mounted. These movements will affect the spatial position (3D calculation) of the birds. The current calculations assume a stable frame of reference, and therefore the associated flight heights have a degree of uncertainty.

Finding the camera orientations and parameters

Spoor estimated the pitch and compass direction of each camera based on landmarks visible in the images .These estimates were confirmed as reasonable by Equinor. Operational engineers from Equinor measured the angles and orientation of the cameras physically with the help of the compass and level on an iPhone. The tilt angles from these measurements correspond well with Spoor’s estimates, but the results from the compass direction did not make sense. The latter might be due to electromagnetic interference from the turbines or incorrect method of measuring. Therefore, the initial compass direction estimates made by Spoor using landmarks were used for the direction of the cameras.

Data transfer

Reducing the transferred data amount

As Figure 20 indicates, data transfer in the winter could be reduced by an additional ~50%, as a lot of the data transmitted had too little daylight to be analysed. A smart system on the sender's side that only sends data with an agreed minimal brightness would be an effective and efficient solution here.

The experiment on frame rate reduction from 30 FPS to 1 FPS showed that the current Spoor AI detection and tracking algorithm needed configuration and training in order to work with 1 FPS. A lower FPS can lead to a loss in bird detections because less data is captured which might not give enough detections of some birds to track them. The exact loss was not identified, because the result of an initial analysis of 50 videos with 1 FPS was that the algorithm needed to be re-trained and optimised for 1 FPS – and this retraining and optimising of the Spoor algorithm was outside the scope of this project. However, the application of the Spoor algorithm is not bound to a particular FPS and will be applicable also for very low frame rates. Continuing to experiment with an intermediate framerate (e.g. 10 FPS) is advisable, as it could yield a good

balance between reducing the transferred data amount and enabling good-quality bird detection and tracking.

Processing data on-site using an edge computer could help to minimise the volumes of data transferred and stored, however, edge computers require direct connection to the camera, as the video stream is routed through the computer for processing before results are transmitted onwards. With pre-installed, multi-purpose CCTV cameras as in this pilot, a number of aspects makes the edge computer option less optimal. Firstly, all videos would have to be streamed through the edge computer, including the HSE/operational videos. Secondly, retrofitting an edge computer takes time. Thirdly, it has a security aspect in the sense that the edge computer would be an external device that is directly connected to the client's internal infrastructure. For these reasons, the edge computer option is not currently recommended for setups with existing CCTV infrastructure installed.

Missing frames in the video stream (data quality)

Some parts of the video stream had missing frames, sometimes over several seconds, and detection and tracking was not possible in these time periods. It is not clear how big a problem this is, and further investigation is required to understand the prevalence and reason for the frame loss.

Video duration (data quality)

36% of the video files received by Spoor had a duration under 2 seconds, rendering them less useful for bird tracking. Spoor requires a minimum of 1 second of a bird being visible, in order to detect it. 2% of the files had 0 seconds of duration, suggesting that something has gone wrong in the writing of the file. The video durations are retrieved by reading the timestamps in the filenames of each video file, and come with the caveat that the timestamp in the filenames could be incorrect.

Analysis of bird observations

Observation rates and activity

Only 12 bird observations occurred during spring. This low number can to a large degree be explained by the low number of analysed hours (46h), as during this period there was only occasional data captured from viewpoint C, and nothing from viewpoints A and B. However, the observation rate per hour recorded was also significantly lower than for other seasons, which might indicate that bird activity was in fact lower during the spring. An important aspect in this regard is the fact that data capture started early May 2023 and ended 10 February 2024 which means that a substantial portion of the spring migration period starting in February-April has not been recorded.

The highest absolute number of observations was 719 and occurred during the autumn, followed by 488 observations during the winter. 236 observations were recorded during the summer, but data from viewpoints A and B was missing for almost half of this period. Looking at the observation rates in Table 4, it is clear that the highest observation rate was during the summer and autumn. The highest number of birds are in general expected to be observed after the breeding season, during late summer and autumn, when the new cohort of birds are added to the flying population. During winter, mortality increases, and the population in spring will therefore be lower. Indeed, the observation rate for the spring is low – almost half that of the summer and autumn. Though as previously mentioned, this could be explained by the low number of analysed hours rather than actual absence of bird activity.

Figure 30 shows the daily observation rates throughout the measurement period. No clear pattern is evident. There are irregular spikes of activity throughout the measurement period. Keep in mind the potential effect of absence of birds detected due to water droplets on the lens/es, which might affect the observation rates and make the results less reliable.

Species identification and occurrence

90% of all bird observations could be classified to species, family or order level, leaving only 10% of all bird observations unidentified to lower taxonomic levels than class. Of the detected species, the white wagtail is the smallest with a wingspan of 25-30 cm, and the Northern gannet is the largest with a wingspan of 165-185 cm. As previously noted, the size of a bird determines the range over which it is visible and detectable, in this case the theoretical detection distance of a northern gannet is 6.4 times higher than that for a white wagtail.

The list of detected species indicates that it is mainly residential birds that are captured by Spoor AI, and not surprisingly the majority of birds detected were seabirds. The exceptions are small passerines, a woodpecker and a raptor, which are migratory birds. The migration period does not seem to significantly affect the detection counts at Hywind Tampen. However, the spread of observed species may be linked to the migration period. Looking at the seasonal distribution of species observations in Table 6, it is clear that the most diverse bird occurrences were during autumn, coinciding with the autumn migration period.

The endangered kittiwake has been verified during the autumn, but this species is notoriously hard to differentiate from other gulls and more kittiwakes could be hidden in the “gull” category.

Distribution of observations across the wind farm

Observations within the wind farm

Viewpoints A and B face almost directly opposite one another and monitor the inner southern area of the wind farm. The approximate distance between the turbines of viewpoints A and B is 2.6 km. As noted in Table 2 and illustrated in Figure 18, the estimated detection range for a bird of 1 m wingspan is ~1.5 km for viewpoint A and ~650 m for viewpoint B. The difference in estimated detection range is explained by the different focal lengths of the cameras. Several of

the observed birds are larger and will therefore be detectable over larger distances, while others are smaller and will be detectable over shorter distances. However, the ranges covered by viewpoints A and B do not overlap (for practical detection purposes), and it is unlikely that the same bird is observed simultaneously from the two different viewpoints.

Observations outside of the wind farm

While viewpoint A and B monitor the inner Southern area of the wind farm, viewpoint C is facing outwards from the wind farm. According to Table 2, the estimated range for a bird of 1 m wingspan is just ~200 m for viewpoint C, which is due to the camera settings. Despite the lower detection range for this viewpoint, it yielded both the largest diversity of species (Table 9) and also the highest overall observation rate (Table 7). The higher species diversity could indicate that more species in fact occur at the perimeter of the wind farm. By closer inspection of Table 8, it is clear that the observation rates do not change much across the seasons, with the exception of spring which had very few collected data points.

Flight directions

Viewpoint A

The majority of the flight direction throughout the measurement period is S/W and N/E, as seen in Figure 37, approximately parallel to the S/W orientation of the viewpoint as visualised in Figure 12.

From Figure 38 it is clear that the summer is somewhat of an exception to the directional pattern, as it displays a more irregular characteristic. As seen in Table 8, the summer data is based on 53 observations, of which 49% – 26 observations – were assigned a direction. The corresponding numbers for autumn and winter are 245 and 133, respectively. Interestingly, it seems that during autumn, birds to a larger degree fly towards west and north, while during winter the flight paths seem to shift towards east and south.

Distinguishing between gulls and non-gulls in Figure 39 shows that the non-gull bird observations display a directionality along the S/W and N/E axis. Just 37 bird observations are the basis for the non-gull directions and this might explain the irregular directional pattern. Still, for both groups the dominating direction is S/W across the full measurement period.

Viewpoint B

The flight directions observed in Figure 40 are mainly along the S/W and N/E axis, not unlike the pattern observed from viewpoint A. These two viewpoints are approximately opposite one another in the wind farm, but as per Table 2, viewpoint B has an estimated detection range for a bird of 1m wingspan of 650 metres, while the corresponding range for viewpoint A was 1,500 m.

The patterns for the winter season for both viewpoints are especially interesting as they both display a reduced directionality in the north and west directions.

Viewpoint C

The dominant direction observed in Figure 43 is along the N/W and S/E axis, perpendicular to the dominant directions from viewpoints A and B. This pattern is consistent across the seasons. Viewpoint C faces S/W out of the wind farm, as opposed to viewpoints A and B which faces “inside” the wind farm. An interpretation of the directionality data of viewpoint C is that birds fly along the periphery of the wind farm and not into it. Of the three viewpoints, viewpoint C had the shortest detection range of ~200 metres for a bird of 1m wingspan (Table 2), so the majority of detection is in the vicinity of the turbine.

Flight altitudes

The lower blade tip height is the vertical distance from the ground or sea up to the lower tip of the rotor blade of the turbine. The lower blade tip height of the Siemens Gamesa SG 8.0-167 DD turbines installed at Hywind Tampen is estimated by Equinor to be 23-24m above the sea. The rotor diameter is 167 metres.

Bird strikes – bird collisions with turbines – are one of the most critical impacts a wind farm can have on birdlife. Empirical flight heights of birds are key to understanding the risk of this impact. Due to the camera orientation and settings, the maximum observable flight heights for a bird of wing span 1 m are ~130 m, ~140 m and ~100 m for viewpoints A, B and C respectively (see Table 2). The viewpoints give good coverage of the air gap between the lower rotor blade tip and the sea.

The flight height flux distribution in Figures 44, 46 and 48 indicates that the majority of the observed birds fly at heights above the air gap, i.e. in the same height as the rotor swept area.

Bird activity correlated to wind conditions

As seen in Figure 50, higher daily observation rates seem to be correlated with lower wind speeds. Meaning, more bird activities at wind speeds below 12 m/s. The same pattern is visible for the hourly observation rates in Figures 51 (gulls) and 52 (non-gulls).

Table 10 shows that overall, the observation rate for this measurement period more than doubles when winds are blowing from north (0.64 birds/hour) compared to south (0.30 birds/hour). Inspecting Table 11, it is clear that the Southerly winds correlate with the lowest observation rates across summer, autumn and winter. The low amount of data collected during spring makes it impossible to conclude on the correlation for this season.

The highest observation rate during summer was for winds blowing from the west (0.99 birds/hour) and the lowest observation rate when winds blew from the south (0.27 birds/hour). During the autumn, the highest observation rates were seen when winds were blowing from the north (0.97 birds/hour). In winter, the observation rates are quite equally distributed across all

wind directions, with a slightly higher observation rate when winds were blowing from the north or the east (0.44 birds/hour).

Reflections and learnings

Spoor believes that empirical and representative facts about bird behaviour are urgently needed to scale the green energy transition in a nature-inclusive way. This pilot has proved that the Spoor software can extract valuable insights from data captured by CCTV cameras that were not originally designated for bird monitoring.

The pilot clearly demonstrates the potential for mutli-purpose use of CCTV cameras. The advantage of using CCTV cameras is that they are often already installed on industrial structures. Retrofitting of equipment can in general be a logistical, practical, financial and bureaucratic challenge, and the use of CCTV cameras circumvents this issue, and therefore fast-tracks results and insights. Considering the results from this pilot, this can be a very efficient way of retrieving high quality bird data for environmental risk management.

Data intake quality monitoring

A key learning from this pilot has been to continue working with the quality of the captured and transferred data, and to develop routines to monitor and alert about deviations. Examples of such deviations are: missing frames in videos, corrupted video files that cannot be opened or have 0 seconds of duration, and obstructions of the field of view by water droplets or other contaminants.

Practical implementation

The collaboration between Equinor and Spoor has been very good, and a key element of this success has been the direct and unobstructed communication especially between technical staff on both sides. Further, Equinor repeatedly made qualified technical staff available, with the right mandate to solve issues as they arose. The support and availability of environmental and biological experts have also been immensely beneficial for execution and implementation.

Equinor programmed the CCTV cameras, set up a data pipeline that handled filtering of HSE from bird monitoring videos, firewall issues and recording times, amongst others. After the initial trial-and-error of the data pipeline setup, the data transfer from Equinor to Spoor worked very well.

For future implementations, it would be beneficial with a site visit early in the project where photos of cameras are taken and measurements (tilt, heading, etc.) are made. Camera parameters (sensor info, zoom, etc.) are crucial information and important to know from the onset of the monitoring. As a more general observation; for future wind farms in development it would be valuable to consider higher resolution CCTV cameras for HSE purposes to allow multi-purpose use for bird monitoring with even higher data quality.

Conclusion

This pilot has demonstrated that CCTV cameras can be used effectively for the combined purposes of HSE/operations monitoring and bird monitoring. It has also delivered insight and learnings that could be implemented along with a roadmap for further development.

Compared to other technologies, multi-purpose use of CCTV cameras is a cost-effective way of collecting valuable, site-specific bird data which allows for more accurate impact assessments – and ultimately, enabling nature and industry to coexist. Based on the technical set-up of the CCTV system, there might be an option to gather unique bird-activity data on several operational assets, building a solid foundation of empirical data to reduce environmental and financial risk over the asset lifetime, and informing the planning and operations of projects currently under development.

Acknowledgements

Spoor wants to particularly thank Kari Mette Murvoll from Equinor for leading the excellent collaboration at every stage of this project. In addition, we are very grateful to Tonje Waterloo Rogstad, Arne Myhrvold and David Cohen for their enthusiasm, creativity and support.

References

- *Artsdatabanken: Norsk rødliste for arter 2021* (2021). Available at: https://artsdatabanken.no/lister/rodlisteforarter/2021 (Accessed: 28 March 2024)
- *Evidently AI: Accuracy vs. precision vs. recall in machine learning: what's the difference?* (n.d). Available at: https://www.evidentlyai.com/classification-metrics/accuracy-precision-recall (Accessed: 28 March 2024)
- *Equinor: Hywind Tampen* (n.d). Available at: https://www.equinor.com/energy/hywind-tampen (Accessed: 28 March 2024)
- *Global Biodiversity Information Facility: What is Darwin Core, and Why does it matter?* (n.d.). Available at: https://www.gbif.org/darwin-core (Accessed: 5 April 2024)
- Hernis (n.d.). PT9W HD IP. Retreived from https://www.hernis.com/docs/dynamic/DSHE097164%20C%20PT9W%20HD%20IP.pdf
- Phillips et al. (2019). "Does perspective matter? A case study comparing Eulerian and Lagrangian estimates of common murre (Uria aalge) distributions. Ecology and Evolution, 9 (8), p.p. 4805-4819. https://doi.org/10.5061/dryad.1hg2n56.
- *The Royal Society for the Protection of Birds: Great Black-backed Gull* (n.d.). Available at: https://www.rspb.org.uk/birds-and-wildlife/great-black-backed-gull (Accessed 28 March 2024)
- *The Norwegian Centre for Climate Services: Observations and weather statistics* (n.d.). Available at: https://seklima.met.no/minutes/wind_from_direction/custom_period/SN76923/en/2023-05-01T00:00:00+02:00;2024-03-28T14:21:59+01:00 (accessed 28 March 2024)
- Zhang *et al.* (2014). An Implementation of Document Image Reconstruction System on a Smart Device Using a 1D Histogram Calibration Algorithm. Mathematical Problems in Engineering. 2014. 1-10. 10.1155/2014/313452.